Chem Soc Rev

Multifunctional Porous Hydrogen-Bonded Organic Framework Materials

Journal:	*Chemical Society Reviews*
Manuscript ID	CS-SYN-02-2018-000155.R2
Article Type:	Review Article
Date Submitted by the Author:	14-Dec-2018
Complete List of Authors:	Lin, Rui-Biao; University of Texas at San Antonio, Department of Chemistry; Sun Yat-Sen University, School of Chemistry and Chemical Engineering He, Yabing; Zhejiang Normal University, Li, Peng; Northwestern University, Department of Chemistry Wang, Hailong; University of Texas at San Antonio, Chemistry Zhou, Wei; National Institute of Standards and Technology, NIST Center for Neutron Research Chen, Banglin; University of Texas at San Antonio, Department of Chemistry

Journal Name

ARTICLE

Received 00th January 20xx,
Accepted 00th January 20xx

DOI: 10.1039/x0xx00000x

www.rsc.org/

Multifunctional Porous Hydrogen-Bonded Organic Framework Materials

Rui-Biao Lin,[a] Yabing He,[a] Peng Li,[a] Hailong Wang,[a] Wei Zhou,[b] and Banglin Chen*[a]

Hydrogen−bonded organic frameworks (HOFs) represent an interesting type of polymeric porous materials that can be self-assembled through H-bonding between organic linkers. To realize permanent porosity in HOFs, stable and robust open frameworks can be constructed by judicious selection of rigid molecular building blocks and hydrogen-bonded units with strong H-bonding interactions, in which the framework stability might be further enhanced through framework interpenetration and other types of weak intermolecular interactions such as $\pi\cdots\pi$ interactions. Owing to the reversible and flexible nature of H-bonding connections, HOFs shows high crystallinity, solution processability, easy healing and purification. These unique advantages enable HOFs to be used as a highly versatile platform for exploring multifunctional porous materials. Here, the bright potential of HOF materials as multifunctional materials is highlighted in some of the most important applications for gas storage and separation, molecular recognition, electric and optical materials, chemical sensing, catalysis, and biomedicine.

1. Introduction

Porous materials or porous media have long been the preeminent platforms for the global scientists and engineers to explore novel multifunctional materials,[1] which are widely applied for filtration, separation, purification, extraction, cooling, drying and catalysis, involving material science, engineering, mechanics, geosciences and biology. Many common substances, such as charcoal, zeolites and ceramics can be regarded as porous media, featuring permanent and interconnected voids of gases/liquids permeability. Zeolites are microporous silicates derived from tetrahedral orthosilicate connected by strong Si-O and Al-O bonds, including over 200 unique zeolite frameworks with Brunauer-Emmett-Teller (BET) surface area of 100–1000 m^2 g^{-1}.[2-4] Zeolite materials have been well explored as commercial adsorbents and catalysts for many important industrial applications on heterogeneous catalysis, gas separation and ion exchange, giving an annual worldwide market of millions tonnes. For instance, synthetic mesoporous zeolites, such as MCM-41, have been widely used as catalysts for fluid catalytic cracking and hydrocracking in the petrochemical industry. It should be noted that zeolites have already made a great impact on the current society.

Other important types of porous crystalline materials including metal-organic frameworks (MOFs)[5] or porous coordination polymers (PCPs),[6,7] covalent organic frameworks (COFs)[8-10] have been emerging over the past two decades. MOFs and COFs are crystalline porous materials that can be straightforwardly self-assembled from various molecular building blocks through strong coordinative or covalent bonds, featuring exceptional porosity, high modularity and diverse functionality.[11,12] The initial efforts to construct coordination polymers with potential open pore structures can be dated back to 1989.[13] However, it took almost one decade to realize the establishment of permanent porosity for the very first MOFs by gas sorption measurements.[14,15] By virtue of secondary building units (SBUs) featuring high rigidity and directionality combining with organic struts, thousands and thousands MOFs with exceptional porosity that far superior to zeolites have been developed, showing BET surface area of 1000–10000 m^2 g^{-1}.[5] The implementation of building blocks approach and isoreticular principle, especially the discovery of open metal sites, to construct functional MOFs further spurred more extensive studies in this field,[16] making it become one of the most rapidly expanding fields among the communities of chemistry, materials science and chemical engineering.[17,18] MOFs have been envisioned as versatile porous materials for gas storage and separation,[19-23] chemical sensing,[24] heterogeneous catalysis[25] and biomedicine.[26,27] In fact, the commercialization of MOFs has been launched by business entities like BASF, NuMat Technologies and MOF Technologies.

---

[a] *Department of Chemistry, University of Texas at San Antonio, One UTSA Circle, San Antonio, Texas 78249-0698, USA. E-mail: banglin.chen@utsa.edu.*
[b] *NIST Center for Neutron Research, National Institute of Standards & Technology, Gaithersburg, Maryland 20899-6102, United States.*

† Footnotes relating to the title and/or authors should appear here.

Electronic Supplementary Information (ESI) available: [details of any supplementary information available should be included here]. See DOI: 10.1039/x0xx00000x

Another type of extended porous frameworks (referred as hydrogen-bonded organic frameworks,[28-32] HOFs), using discrete organic molecules to self-assemble via intermolecular hydrogen-bonding interactions, have also been proposed as potential porous materials more than two decades ago. The inherent features of H-bonding connections (weak, flexible, poorly directional, and reversible) render HOFs have some intriguing differences from zeolites, MOFs and COFs, such as solution processability and characterization, easy purification and healing by simple recrystallization. Although the initial studies to construct HOFs with guest inclusions have been presented since the early 1990s,[33-50] it was not until 2010 that examples of HOFs with permanent porosity established by gas sorption isotherms have been reported.[28,51] Similar but shorter development process can be found as looking back the early stage of exploring MOFs with permanent porosity in the 1990s.[13-15] Based on the pioneering work on the construction of extended organic networks by Wuest and others,[33-50] we demonstrated the permanent porosity of HOFs for their potential applications in gas separation. It is well understood that the activation of HOFs is more challenging than those of other porous frameworks including MOFs if taking the labile nature of H-bonds into account, as they are indeed much weaker than the covalent and coordinative ones. The removal of included guest molecules typically results in denser isomers, so most organic extended frameworks are not sufficiently robust to retain porosity upon guest removal. Only HOFs featuring rigid and directional building units can be demonstrated to show permanent porosity. Therefore, the establishment of permanent porosity for HOFs represented a turning-point in this field. By virtue of rigid backbones, the record of BET surface area for HOFs reached to over 2700 m^2 g^{-1} by Oppel in 2012,[52] and exceeding 3400 m^2 g^{-1} as the nowadays benchmark.[53] The implementation of high porosity of HOFs imparted momentum to the development of multifunctional HOFs and spurred interest in exploitation of new HOFs with recorded porosity. To date, HOFs have shown great potential as versatile platform to explore novel porous materials for gas storage and separation, molecular recognition, conductive and optical applications, heterogeneous catalysis, and biomedicine.

Since the early development of hydrogen-bonded organic frameworks, the scope for this type of porous materials has broadened rapidly, in terms of structures and applications. It is now timely to reassess HOFs, not as a new area but as a more mature field. In this Review, we focus on selected HOFs materials as examples to provide broader concepts for readers who are new to this field. We discuss the unique features that set HOFs apart from other porous frameworks. We highlighted the progresses on some of the most important applications of HOF materials.

2. Chemistry of HOFs

HOFs are assembled by organic molecules based on certain H-bonding interactions. Compared to covalent linkages (B–O, C–N, C=N) in COFs, coordination bonds (M–O, M–N) in MOFs, Si–O and Al–O in zeolites, hydrogen bonds in HOFs are relatively weak, which enables reversible reactions occur during the crystallization of HOFs, giving highly crystalline. But the other side of the coin is that challenges lie in the construction of stable, rigid and permanently porous HOFs. Several approaches have been successfully applied for the concerns involving polymorph problem during crystallization, functional sites, and framework stability after guest removal and establishment of porosity.

2.1 Conceptual basis.

The prototypical H-bond refers to interaction between two water molecules ($O^{\delta-}–H^{\delta+}\cdots O^{\delta-}$), which can be further extended to other systems including hydrogen atom between two electronegative atoms ($X^{\delta-}–H^{\delta+}\cdots Y^{\delta-}$, X, Y mainly O, N, F). According to the IUPAC definition,[54] the hydrogen bond is *an attractive interaction between a hydrogen atom from a molecule or a molecular fragment X–H in which X is more electronegative than H, and an atom or a group of atoms in the same or a different molecule, in which there is evidence of bond formation*. Hydrogen bonded organic frameworks are defined as frameworks connected through H-bonding interactions between the organic units including both pure organic and metal-containing organic moieties (Table 1 and Fig. 1),, which can be further enforced by other weak interactions such as the C–H⋯π interactions, van der Waals interactions, dipole–dipole interactions, halogen bonds, the cation⋯π interactions and so on.[55]

Table 1 Criteria for H-bonds adapted from Steiner and Jeffrey.[55]

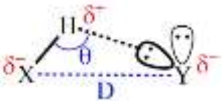	Strong	Moderate	Weak
D/Å	2.2-2.5	2.5-3.2	>3.2
H⋯Y/Å	1.2-1.5	1.5-2.2	>2.2
θ/°	170-180	>130	>90
X-H *vs.* H⋯Y	X-H ~ H⋯Y	X-H > H⋯Y	X-H >> H⋯Y
Bond energy/kJ mol^{-1}	63-167	17-63	<17

The H-bond energies in most systems usually are within 10–40 kJ mol^{-1}, which extend to 1–170 kJ mol^{-1} considering other extreme cases, but still lower than those of coordination bonds (90–350 kJ mol^{-1}) and covalent bonds (300–600 kJ mol^{-1}).[8] Hence, the rigidity and directionality of H-bond are lower than coordination bond and covalent bond, which makes rational design of extended framework more challenging. According to several criteria including the bonding energies of H-bonds, these interactions were proposed to be catalogued into weak, moderate and strong H-bond. In terms of constructing stable and rigid HOFs, only relatively strong H-bond interactions are feasible, as labile H-bonds may lead to polymorph problem, flexibility or framework collapse after desolvation. Weak H-bonds feature long bonding distances and poor directionality, giving different polymorphs with negligible thermal energy difference. Given that close-packed structures are thermodynamically favoured, once the kinetically formed open structures cannot be stabilized by H-bond interactions, any external stimulus like vacuum would lead to their solid-state transformations to dense structure. Therefore, applying weak H-bond for HOFs construction can be problematic, and make it more complicated.

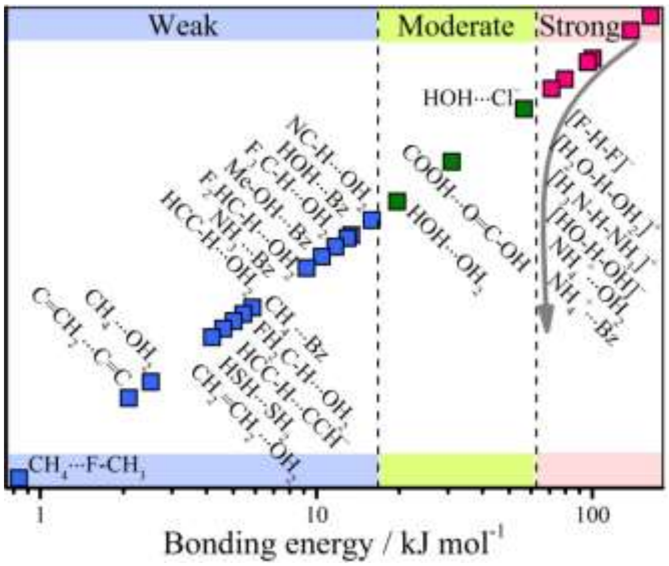

Fig. 1 Various types of hydrogen bonds. This sketch is not exactly quantitative but the coloring attempts to give a visual scale of bonding energies. Data from Steiner's paper.[55]

On the other hand, highly directional and strong H-bonds, mainly intermolecular O/N–H···O/N interactions, often dominate and widely exist in many supramolecular systems. Based on detailed analyses of crystal structures from the Cambridge Structural Database (CSD), O–H···O interactions from nearly 140000 structures show mean bonding distance of 2.77 Å, while N–H···O interactions from nearly 120000 structures show that of 2.88 Å (Fig. 2). The stronger H-bond with shorter bonding distance is accompanied by a better directionality (i.e. bond angle, distribution centred at 171° vs 168°). From the perspective of rational design, compared to weak H-bond, highly directional and strong H-bond interactions help simplified the chemistry of extended network from self-assembly of organic molecules.

Although discrete organic compounds especially cage like molecular can also exhibit intrinsic, shape-persistent voids, the absence of distinct intermolecular H-bonds makes these porous molecules zero-dimensional, suffering from polymorphism upon aggregation. This class of compounds has long been developed as porous solids, e.g. tris(*o*-phenylenedioxy)cyclophosphazene (TPP),[56-59] Dianin's compound,[60-62] calixarenes,[63-68] cucurbiturils,[69,70] Noria,[71] series of imine cages,[72-74] and so on.[75-79] Actually, porous organic cages are unique for their intrinsic porosity that exists even under discrete state,[80] which renders them as another type of porous organic solids.[81]

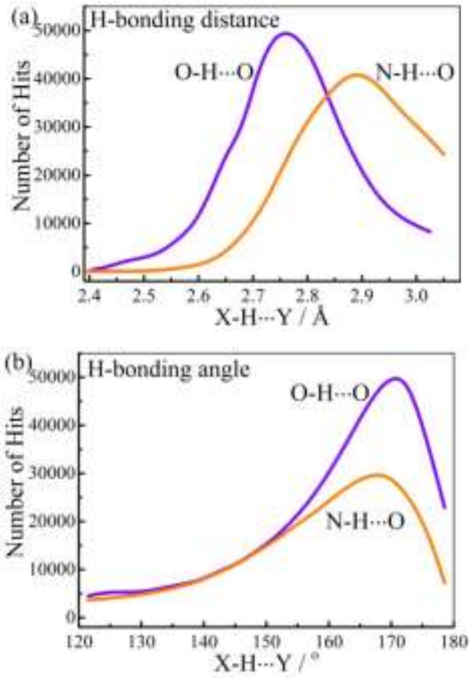

Fig. 2 Distributions of (a) O–H···O and N–H···O bond-length and (b) corresponding directionality, based on analyses of crystal structures from the Cambridge Structural Database with updates by August, 2018. Structures got from the database was applied with a bonding cutoff of 3.04 (for O–H···O) and 3.07 Å (for N–H···O), i.e. the sum of van der Waals radii. The bond angle cutoff is >120°.

Taken the above together, we here give a working definition for HOFs in this article, that porous crystals of extended structures compose of organic molecular building units, and moderate to strong H-bonds linkage that specifically involves the H-atom. In most cases, HOFs mainly feature nitrogen or oxygen moieties as donors or acceptors for highly directional H-bonding.

2.2 General design principle.

The basic concerns for constructing HOFs by rational design should focus on the porosity, framework rigidity and material stability. In this regard, certain approaches demonstrated in the constructions of other crystalline materials might be applicable to HOFs synthesis. But, the intrinsic natures of organic molecules with corresponding H-bonding make the self-assembly of HOFs more complicated. Accordingly, the design principles for HOFs synthesis need extra insights. Moreover, additional concerns for constructing HOFs with functional sites should also be taken into account.

Given the diversified organic groups of H-bonding potential, many molecular moieties can be applied for H-bonding interactions (Fig. 3), including carboxylic acid,[82-87] pyrazole,[88] 2,4-diaminotriazine,[89,90] amide,[91] benzimidazolone, imide, imidazole, amidinium,[92] boronic acid,[42] resorcinol,[38,93] pyridine, 2,6-diaminopurine,[94] and so on.[95,96] It should be noted that, owing to the flexible nature of H-bond, these organic groups can give enormous polymorphs by rational assembly in different geometry. But only energetically favourable frameworks can be crystallized from molecular building blocks. Cooper and Day *et al.* presented a good example to identify highly porous HOFs with high performance for target applications, by using energy–structure–function maps of vast computational crystal structures.[53] Their work demonstrated that the experience and principles succeed in MOFs and COFs cannot simply be applied to the design of HOFs.

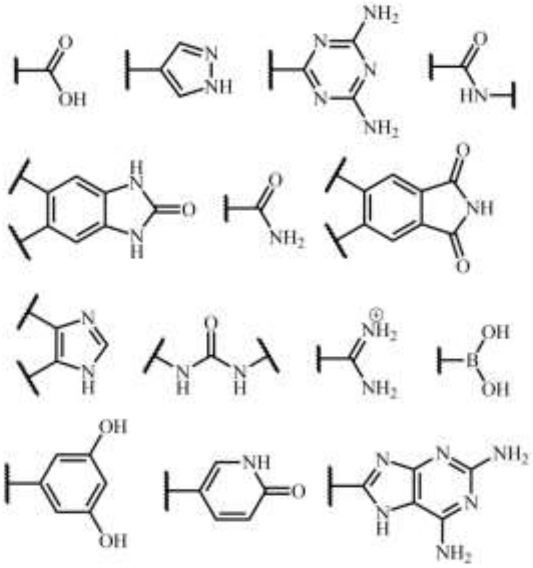

Fig. 3 Various O/N containing organic groups for potential H-bonding units, including carboxylic acid, pyrazole, 2,4-diaminotriazine, amide, benzimidazolone, imide, imidazole, amidinium, and so on.

In principle, organic groups with an equal number of H-bonding donors and acceptors are more suitable for HOFs generation. Because, these H-bonding donors/acceptors can distinctly form into certain inherent H-bonding units, which can be dimers, trimers, and even chain structures (Fig. 4). Apparently, the H-bond building units are more rigid and directional than single H-bonding donor/acceptor pairs, which facilitate the construction of HOFs. Therefore, combined H-bond building units with suitable organic backbones (Fig. 5), expanded frameworks with various topologies and pore structures can then be generated. It should be noted that the concept of H-bonding units is critical for the construction of HOFs with higher porosity, as its geometry can be transmitted into the net while the length of organic backbones usually dominate the pore size. Actually, certain isoreticular series of HOFs can be generated based on isomorphic organic molecules of different length via same connection style. For instance, H-HexNets HOFs from a series of C_3-symmetric hexacarboxylic acids,[97-102] fluorinated trispyrazole HOFs,[88,103] and tribenzimidazolone HOFs have been successfully synthesized.[52,53] Besides single-component HOFs, there are also few examples about mixed-ligands approach to construct porous HOFs,[104-106] as exemplified by SOF-7,[107] guanidinium–sulfonate salts,[108] ammonium–sulfonate salts (Fig. 5),[109] which is more challenging. But the implementation of such approach can reap community of this field to construct diverse porous materials.

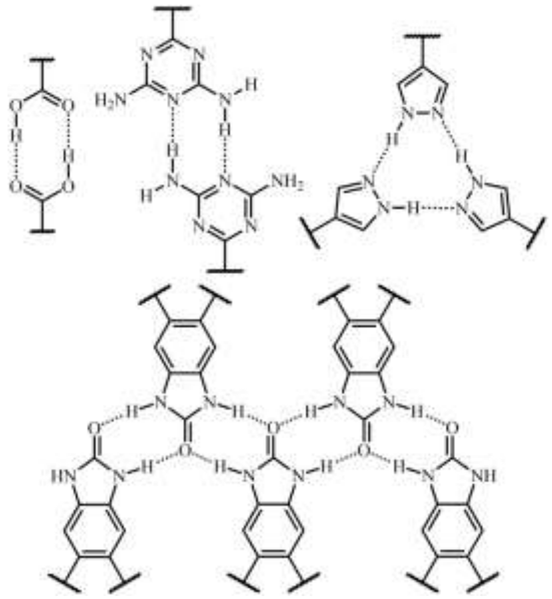

Fig. 4 The geometry of typical H-bonding units assembled from common organic groups through multiple intermolecular H-bonds, serving as the building blocks for HOFs construction.

In fact, with the template effect of guest molecules, the theoretic porosity of HOFs can reach extremely high, even for those porous solid featuring very weak intermolecular interactions. But, in most case, the open framework cannot be well retained after guest removal owing to the fragile connections. To generate HOFs with high stability and framework rigidity, several approaches as listed below can be employed. (a) Get stronger intermolecular interactions involved during the molecular assembly to HOFs. To achieve so, multiple H-bonding interactions between organic ligands, or charge-assisted H-bonds between cations and anions especially high-charged ionic ones are favourable for constructing stable HOFs. Therefore, multi-branched organic molecules would be very promising candidates. For charged H-bond, the acidity and basicity of involved ligands are proposed directly related to the H-bonding strength.[109] The combination of strong acid and strong base can result in high permanent porosity. (b) Employ rigid organic ligands with stereoscopic backbone for HOF construction. Although the linkage of H-bonded units in most of porous organic solids featuring weak H-bonds might be sensitive to desolvation, some of these supermolecular frameworks still can exhibit permanent porosity, which originated from insufficient intermolecular stacking owing to the stereo-steric effect. For example, Aida and Yamagishi *et al.* reported a porous molecular crystal from the assembly of polypyridine molecules through extremely weak C–H···N interactions, yet showing thermally stable porosity with a BET surface area of 219 $m^2\ g^{-1}$.[110] (c) Introduce suitable interpenetrations into the HOFs. It is well known that interpenetration would reduce the pore size but can stabilize open framework. This is because interpenetrated frameworks is of a lower energy and thermodynamic favorable. Interpenetration can be readily realized for suitable H-bonded frameworks like polycarboxylic acid by controlling their crystallization conditions involving changes on solvents and/or

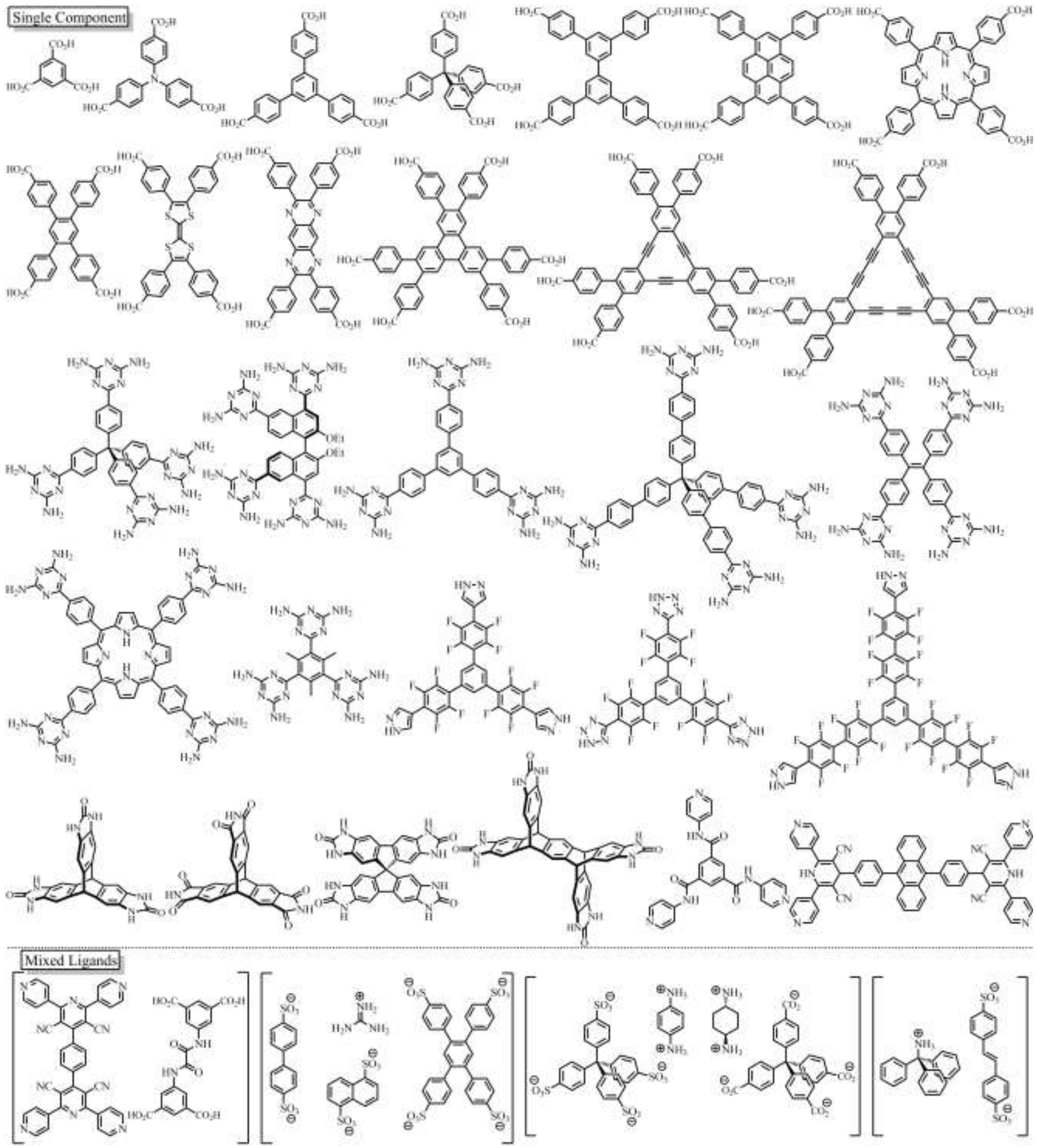

Fig. 5 Schematic representation of various organic ligands for the construction of HOFs. Roughly categorized based on the types of components.

temperatures. (d) Get extra intermolecular interactions like π-π stacking and van der Waals forces involved for stable HOFs construction. It should be noted that intermolecular interactions like π-π stacking are important driving force for other stable and rigid organic porous solids, especially for two dimensional COFs, which usually contain π-conjugate systems. Actually, the existence of aromatic moieties enhances the chemical resistance for solvents, acids and bases owing to their inert reactivity. Thus, large planar aromatic molecules should be employed for constructing stable HOFs. (e) Avoid forming any terminal H-bonding donor and acceptor, as they may interact with polar solvent molecules, which raises up the activation challenge and complexity. Therefore, if possible, large polar and high boiling point solvents should also be avoided during the synthesis of HOFs.

In short, based on the combination of directional H-bond building units with rigid organic backbones, highly porous HOFs featuring strong intermolecular interactions can be realized to show permanent porosity, in which the architectural stability plays an important role.

2.3 Stability of HOFs.

The structure stability is another important prerequisite for HOFs to exhibit permanent porosity. In terms of thermal and chemical stability, HOFs are comparable to MOFs and COFs. HOFs also exhibit additional unique feature. For example, the healing of collapsed HOFs can be readily realized by simple recrystallization,[111,112] as their bonding manners are relatively reversible.

Water stability is very important aspect that needs to be considered for applying porous materials in practical processes.[11,113] In this context, many HOFs show remarkable water stability owing to the insolubility of organic ligands in water, and the hydrophobic nature of pure organic moieties, especially that of aromatic groups. In contrast, many MOFs are sensitive to humidity or water, as water molecules are good alterative ligand toward metal ions.[114]

It should be noted that HOFs often subject to poor stability for highly polar organic solvents like dimethyl sulfoxide. This is because solvents of high polarity usually are good H-bonding donors/acceptors, which can form strong H-bonds with the organic ligands, resulting in the leaching and etching of organic molecules from HOFs. But the good reversibility of H-bonding enables the recrystallization to original HOFs after the removal of binding solvent molecules. Hence, HOFs show good solution processability, and can be easily regenerated. Also, besides in common organic solvents, some types of HOFs like carboxylic acid can even stable in acid.[115]

Compared to zeolites, MOFs and COFs, the aforementioned bonding interactions in HOFs are somewhat flexible and weak,[8] thus showing relatively low architectural stability. Nevertheless, increasing the coplanarity and/or geometric rigidity of H-bonding units can give relatively rigid HOFs with permanent porosity.

2.4 Permanent porosity in HOFs.

Permanent porosity is a direct target from constructing HOFs, which is essential for other further applications. Since crystalline organic supermolecular solids with open framework were constructed in the 1990s,[33-50] the establishment of microporosity with surface area and pore volume determination has been long-standing challenges. As mentioned, most open framework in HOFs would not give effective permanent porosity in the absence of guest molecules, owing to the fragile nature of H-bonds. Therefore, the guest removal of this type of porous materials needs to be performed under mild conditions. On the other hand, suitable strategies listed in section 2.2 can be employed to construct relatively robust HOFs. The implementation of establishing permanent porosity was achieved until the early 2010s.[28,51] To date, although lots of organic extended frameworks have been reported, only a few dozen HOFs can exhibit microporosity with surface area (Table 2-3).[116-120] Except for some robust HOFs, guest removal under vacuum with direct heating is too harsh for most labile HOFs, which would lead to corresponding collapse. To facilitate activation under mild condition, solvent-exchanging of solvent molecules of high boiling-point to volatile ones seems a feasible approach.[52,53] However, many HOFs are subject to certain solubility in common exchanging solvents, which are not applicable for solvent exchange. Therefore, the development of HOFs is significantly lagged behind that of other porous materials including MOFs and COFs. Hence, more suitable activation strategies are required for labile HOFs to show porosity, which need continuous intensive endeavors.

Additionally, HOFs can be easily crystallized through solution evaporation/cooling, liquid/vapor diffusion, sublimation,[88] and even solvothermal method[121] that frequently applied for MOFs. Since HOFs can be subject to polymorph issue, their crystallization is sensitive to solvents, templates, concentrations, temperatures and so on, giving kinetic and thermodynamic products.[53] In principle, crystallization at high concentrations or for short reaction time might give kinetic isomers. To obtain thermodynamic phase, it is better to slow down the rate of crystallization or to increase the thermal energy for overcoming barriers of activation energy between various isomers (i.e. at high temperatures). The application of solvothermal method represents a good step in this field, as it provides a feasible approach to assembly stable HOFs.

Overall, to obtain HOFs with accessible porosity for further applications, organic frameworks based on H-bonds can be successfully constructed based on framework chemistry. The architectural stability is important for HOFs to show permanent porosity, whereas the guest removal of HOFs does great matter for them to serving as porous materials.

Table 2 Summary of porosity and functionality in single-component and permanently porous HOFs (until October 2018).

Types	HOFs	Formula	Void/%	Pore size/Å	S_{BET}/m^2 g^{-1}	Functionality	Ref.
DAT derivatives	HOF-1a	$C_{37}H_{32}N_{20}$	42	~8.2	359	C_2H_2/C_2H_4 (56/3.9)^e	28
	HOF-2a	$C_{36}H_{34}N_{20}O_2$	54.3	~4.8	238	Separation of chiral secondary alcohols	138
	HOF-3a	$C_{33}H_{27}N_{15}$	75	~7	165	C_2H_2/CO_2 (47/21)^e	133
	HOF-4a	$C_{61}H_{48}N_{20}$	42.5	3.8 × 8.1	312	C_2H_4/C_2H_6 (11/3.6)^e	117
	HOF-5a	$C_{38}H_{32}N_{20}$	41.1	~3.9 × 5.5, ~3.9 × 6.8	1101	CO_2/CH_4 (90/-)^e, CO_2/N_2, and C_2H_2/CH_4 (102/-)^e	130
	HOF-6a	$C_{56}H_{42}N_{24}$	63.4	~6.4, ~7.5	130	Proton conduction, CO_2/N_2	145
	HOF-7a	$C_{56}H_{42}N_{24}OZn$	-	3.2 × 4.7, 4.2 × 6.7	124	CO_2/N_2 (11/-)^e	131
	HOF-9a	$C_{56}H_{42}N_{24}OZn$	-	3.2 × 4.7, 4.2 × 6.7	124	Py/BTX, CO_2/N_2 (40/6)^e	132
	HOF-10a	$C_{56}H_{42}N_{24}OZn$	55	3.2 × 4.7, 4.2 × 6.7	187	Fluorescence Ag$^+$ sensing	154
Carboxylic acid	IISERP-HOF1	$C_{21}H_{15}NO_6$	~34	9.1 × 9.4^a	412	CO_2/N_2 (65/-)^e	121
	HOF-11		33.2	6.2 × 6.8	687	CO_2/CH_4, CO_2/N_2 (30/2)^e, and C_2H_2/CH_4 (45/8)^e	123
	Tcpb/H_3BTB	$C_{27}H_{18}O_6$	38	18.5^c	1095	CO_2 and H_2 adsorption	134
	HOF-BTB			12/16.6^c	955	C_2H_2/CH_4 (64/8.7)^e, C_2H_4/CH_4, and C_2H_6/CH_4	136
	HOF-TCBP	$C_{40}H_{26}O_8$	56	17.8 × 26.3	2066	C_3/CH_4 and C_4/CH_4	112
	PFC-1/H_4TBAPy	$C_{44}H_{26}O_8$	-	18 × 23	2122	Chemo-photodynamic therapy	115
	CoTCPp	$C_{72}H_{44}N_4O_{12}Co$	~19	4.0 × 6.5	98	Alkylbenzene oxidation	160
	TCF-1	$C_{29}H_{20}O_8$	17.3	2.9 × 5.5 to 4.2 × 6.4	-	CO_2, CH_4, and C_6H_6 adsorption	119
	Tp-1	$C_{60}H_{36}O_{12}$	54	~11, 15.8^a	788	Fluorescence and hydrocarbon adsorption	97
	T12-1	$C_{66}H_{36}O_{12}$	41	~11, 4.6 × 15.8^a	557		
	T18-1	$C_{72}H_{36}O_{12}$	58	~11, 7.1 × 15.8^a	-		
	Ex-1	$C_{90}H_{48}O_{12}$	59	~11, 11.4 × 15.8^a	-		
	TpMe-1	$C_{72}H_{60}O_{12}$	45.2	6.4	561	Fluorescence	151
	TpF-1	$C_{60}H_{24}F_{12}O_{12}$	50.4	14.5	219		
	CPHAT-1a	$C_{72}H_{44}N_4O_{12}$	31	6.4	649^b	Fluorescence	98
	CBPHAT-1a	$C_{72}H_{44}N_4O_{12}$	45	14.5	1288	Fluorescence	99
	PETHOF-1	$C_{62}H_{38}O_{12}$	80	~11^c	1150	CO_2/CH_4 (32.6/10.6)^e	85
	PETHOF-2	$C_{62}H_{38}O_{12}$	49	~11^c	1140	CO_2/CH_4 (43.4/4.2)^e	
Azole derivatives	Trispyrazole 1	$C_{33}H_{12}F_{12}N_6$	56	16.5	1159	Fluorocarbons hydrocarbon adsorption	88
	Trispyrazole 16	$C_{30}H_9F_{12}N_9$	-	18	903	-	103
	Tristetrazole 23	$C_{27}H_6F_{12}N_{12}$	-	11.9	222	-	
	Trispyrazole 25	$C_{51}H_{12}F_{24}N_6$	58.1	26.4	1821	-	
	benzotrisimidazole	$C_{12}H_3F_9N_6$	21.7	2.9 × 4.6	131	O_2/Ar, O_2/N_2	137
	FDM-15	$C_{23}H_{14}N_6$	-	~11.5	749	*p*-xylene/C_8H_{10}, C_{60} capture	139
Amide derivatives	TTBI	$C_{23}H_{14}N_6O_3$	60	14.5, 3.8 ×5.8	2796	CO_2 and H_2 adsorption	52
	T2-β	$C_{23}H_{14}N_6O_3$	-	-	1665	CH_4 storage, C_3H_8/CH_4	53
	T2-γ	$C_{23}H_{14}N_6O_3$	-	19.9	3425		
	T2-δ	$C_{23}H_{14}N_6O_3$	-	-	365		
	NPSU-3	$C_{46}H_{60}N_6O_5$	16.1	10.8	29	Organic dyes adsorption	144
Pyridine derivatives	HOF-8	$C_{24}H_{18}N_6O_3$	24	4.5 × 6.8	-	CO_2/N_2, CO_2/H_2 and C_6H_6 adsorption	91
	SOF-1a	$C_{60}H_{36}N_{10}$	34	~7.8	474	CO_2 and C_2H_2 adsorption	51
Benzoin	Cyclotetrabenzoin	$C_{32}H_{24}O_8$	10	-	42	CO_2 and H_2 adsorption	118
Porous Molecular Solids	CB[6]	$(C_{36}H_{36}N_{24}O_{12})\cdot 2H_2O$	14.4	6	210	C_2H_2 adsorption	70
	TTP	$C_{18}H_{12}N_3O_6P_3$	25	4.6	240^{d,59}	CO_2 and CH_4 adsorption	58
	CC3	$C_{72}H_{84}N_{12}$	-	5.8, 7.2	624	CO_2, CH_4 and H_2 adsorption	72
	TBC[4]DHQ	$C_{38}H_{44}O_6$	-	2.2, 11.2	230	CO_2 adsorption	67

[a] Distance of atom centers including vdW radii. [b] Estimated by PLATON. [c] Pore size distribution from 77 K N_2. [d] Langmuir surface area. [e] The adsorption amount (cm^3 g^{-1}) at room temperature and 1 bar are presented in parentheses.

Table 3 Summary of porosity and functionality in mixed-ligands and permanently porous HOFs.

Types	HOFs	Formula	Void/%	Pore size/Å	S_{BET}/m^2 g^{-1}	Functionality	Ref.
Pyridine-carboxylic derivatives	SOF-7a	$(C_{40}H_{20}N_{10})(C_{18}H_{12}N_2O_{10})$	48	13.5 × 14.0	900	CO_2/CH_4	107
	SOF-9a	$(C_{44}H_{22}N_{10})(C_{30}H_{18}O_8)$	34.2	12.0 × 12.3	181	CO_2/CH_4, CO_2/N_2	120
	SOF-10a	$(C_{44}H_{22}N_{10})(C_{18}H_{12}N_2O_{10})$	29.9	12.1 × 14.2	221		
Ammonium sulfonate derivatives	HOF-GS-10	$(CH_6N_3)_2(C_{10}H_6O_6S_2)$	16	3.9 × 5.7	-	Proton conduction	146
	d-POS-1	$(C_{19}H_{18}N)_2(C_{12}H_{10}O_6S_2)$	31.5	5.9 × 7.0, 9.1 × 10.4	398	Fluorescence sensing	116
	CPOS-1	$(C_6H_{16}N_2)_2(C_{25}H_{16}O_{12}S_4)$	-	-	216	Proton conduction	109
	CPOS-2	$(C_6H_{10}N_2)_2(C_{25}H_{16}O_{12}S_4)$	-	-	129		
	CPOS-3	$(C_{12}H_{14}N_2)_2(C_{25}H_{16}O_{12}S_4)$	-	-	12		
	CPOS-4	$(C_6H_{16}N_2)_2(C_{29}H_{16}O_8)$	-	-	29		
	CPOS-5	$(C_8H_{12}N_4)_2(C_{25}H_{16}O_{12}S_4)$	14.6	5.3 × 6.8	-	CO_2/CH_4, CO_2/N_2	147

3. HOFs for gas storage and separation

The establishing of permanent porosity enables HOFs to serve as novel porous media for the enrichment of gas molecules. The confined pore spaces in HOFs are suitable to capture or encapsulate various important gas molecules, including H_2, N_2, O_2, CO_2, CH_4, C_2H_2, C_2H_4, C_2H_6, and so on. In particular, as HOFs are composed of light elements (mainly C, H, N and O) and with high surface areas, their high gravimetric uptake capacities for gases can be expected. On the other hand, highly selective separation of gas molecules based on HOFs can also be realized via precise control of their pore size.

3.1 Gas storage

Portable storage and delivery of gases in a convenient, cheap and safe way is very challenging, especially for energy gases like H_2 and CH_4. In specific, methane (main component of natural gas) is highly attractive as clean fuel considering its natural abundance and low carbon dioxide emission. The potential of hydrogen-bonded framework for CH_4 storage is well demonstrated by a potentially important future fuel source, methane clathrate (or natural gas hydrate),[122] which is a solid similar to ice featuring a large amount of CH_4 trapped by water molecules (Fig. 6). One volume of fully saturated hydrate would dissociate to about 180 volumes (STP) of CH_4, corresponding to about 15 wt% (by mass). But reversible and rechargeable storage under mild conditions is more desirable. Given that HOFs show larger surface areas and lower densities, it may be promising to apply these materials for gas storage. HOFs have exhibited high storage capacities for certain important gases such as hydrogen, methane, and carbon dioxide, even at ambient temperature.

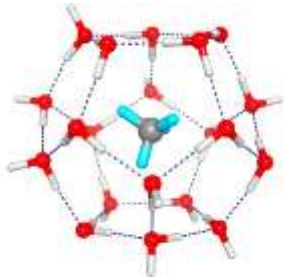

Fig. 6 The cage structure of methane clathrate (Structure I). Structure from Ojamäe.[122]

The potential of HOFs for gas storage has been proven right after the discovery of their permanent porosities. In 2010, Schröder *et al.* reported a stable HOF $(C_{60}H_{36}N_{10})\cdot 2.5DMF\cdot 3MeOH$ (SOF-1; $C_{60}H_{36}N_{10}$, 9,10-bis(4-((3,5-dicyano-2,6-dipyridyl)dihydropyridyl)phenyl)anthracene) showing high gas uptake capacities for CH_4, C_2H_2, and CO_2 (Fig. 7).[51] In this HOF, the bulky dihydropyridyl ligands assemble via multiple strong hydrogen bonds (N–H···N 2.87 Å), forming layered networks, which further stack to 3D structure through weak C–H···N and π···π interactions. The 1D pyridyl-decorated channels along crystallographic [010] axis in SOF-1 is ~7.8 Å, with solvent-accessible voids ~34.0% of the total cell volume. The activation of SOF-1 at 403 K gave SOF-1a, and its decomposed temperature is at >673 K. Interestingly, the desolvated SOF-1a showed temperature-dependent porosity, with a significant adsorption increasing for N_2 at from 77 K to 125 K, implying certain framework flexibility. The BET surface area of SOF-1a was estimated to be 474 m^2 g^{-1} based on N_2 isotherm at 125 K (143 cm^3 g^{-1}). SOF-1a shows considerable methane uptake at 10 bar and 195 K of 106 cm^3 (STP) g^{-1}. SOF-1a also absorbs large amount of C_2H_2 (124 cm^3 g^{-1}) at 1 bar and 195 K. At ambient temperature, SOF-1a shows certain uptake capacity for CO_2 (69 cm^3 g^{-1}) at 16 bar and 298 K. The storage performance of SOF-1a is superior to those of many crystalline molecular organic solids owing to its high porosity/surface area. In additional, SOF-1a exhibits certain selective adsorption over different gases.

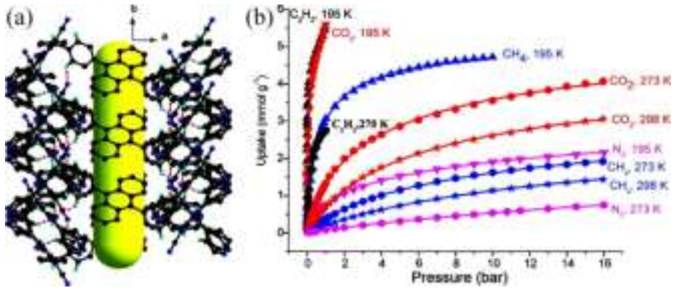

Fig. 7 (a) The 3D porous structure of SOF-1 with 1D channels. (b) Comparison of gas adsorption on SOF-1a. C_2H_2 (black), CO_2 (red), CH_4 (blue), and N_2 (magenta) at 195 K (triangles), 270 (or 273) K (circles) and 298 K (stars). Reprinted with permission.[51] Copyright 2010 American Chemical Society.

A very efficient approach for boosting the gas storage capacity of HOFs is to increase their porosity and surface area. In 2012, Mastalerz and Oppel synthesized a highly porous HOF triptycene trisbenzimidazolone ($C_{23}H_{14}N_6O_3$, TTBI) with exceptional surface area (Fig. 8).[52] In this HOF, the benzimidazolone units are assembled into ribbon-like structures through multiple H-bonding (N–H···O 2.74 and 2.88 Å), giving a 3D framework with 1D cylindrical (14.5 Å) and slit-like channels (3.8–5.8 Å). The solvent-accessible void of this HOF is ~60% of the total cell volume. The desolvated TTBI is permanently porous, showing an experimental BET surface area of 2796 m^2 g^{-1}. Such high porosity enables this HOF to show significant H_2 uptake at 1 bar and 77 K of 243 cm^3 (STP) g^{-1} (2.2 wt %), which is even comparable to those for some well-known MOFs with open metal sites (e.g. Mg-MOF-74, 2.2 wt % H_2) under the same condition. This TTBI HOF also shows a large uptake capacity for CO_2 (80.7 cm^3 g^{-1}, 15.9 wt %) at 1 bar and 273 K.

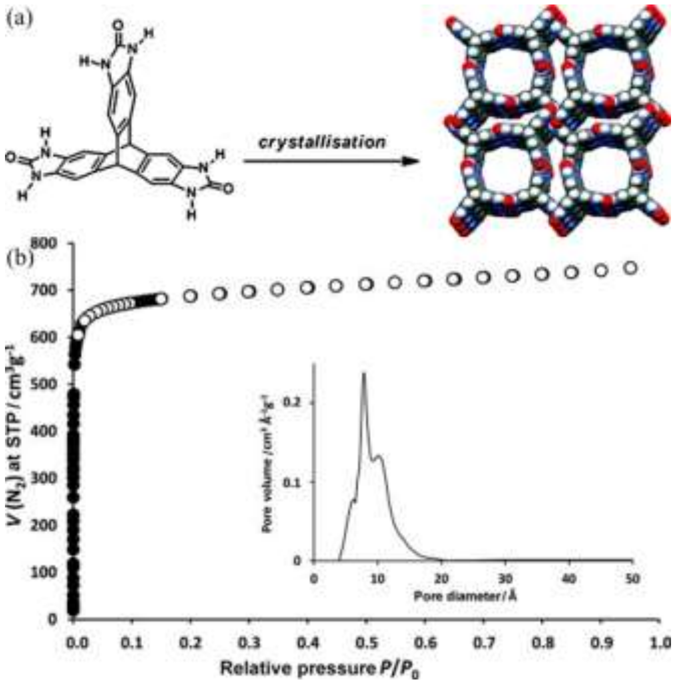

Fig. 8 (a) Schematic diagram about structure of triptycene trisbenzimidazolone (TTBI). (b) Nitrogen sorption isotherm of activated TTBI at 77 K. The inset shows the measured pore-size distribution. Reproduced with permission.[52] Copyright 2012 Wiley-VCH.

To discover HOF with higher porosity, Day *et al*. reported an impressive way via building energy–structure–function maps to identify highly porous HOFs, which is based on the combination of computational framework structure prediction and properties prediction.[53] Lattice energy surface analyses for several expanded benzimidazolone and imide molecules were carefully conducted. Multiple high-porous and low-density framework structures that are superior to the above TTBI HOF (T2-α in this work) can be targeted from substantial predicted polymorph structures (Fig. 9). Among these structures, a new large-pore polymorph T2-γ of TTBI HOF was predicted to be a superior HOF for methane storage, which was verified by further crystallization of ($C_{23}H_{14}N_6O_3$)·7.79DMA (T2-γ) and corresponding sorption experiments. Benzimidazolone T2-γ contains hexagonal pore channels with exceptional diameter of 19.9 Å, showing the lowest density (0.412 g cm^{-3}) of any reported molecular solid. The experimental BET surface area was estimated to be 3425 m^2 g^{-1}. The saturation CH_4 uptake capacity at 115 K for T2-γ was measured to be 47.4 mol k g^{-1} (437.4 v (STP)/v). Small-pore and denser polymorphs T2-β and T2-δ were also realized for related hydrocarbon separation. Furthermore, by applying such approach of energy–structure–function maps, an extended benzimidazolone analogue ($C_{35}H_{20}N_6O_3$)·17.3DMF (T2E-α) was obtained, showing a hexagonal pore channels of 28 Å in diameter, which is the largest pore size observed for any HOFs so far.

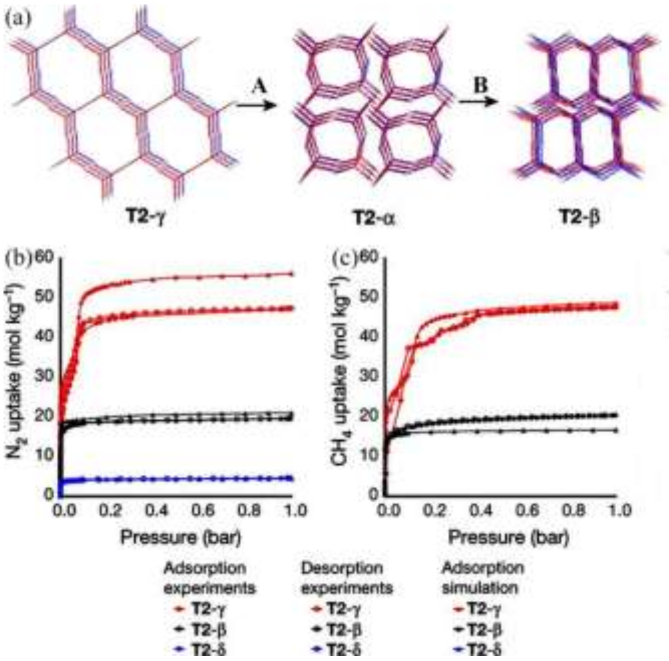

Fig. 9 Crystal structures and gas adsorption isotherms for polymorphs of T2. (a) Overlays of predicted (red) and experimental (blue) structures for T2-γ , T2-α and T2-β , ordered by increasing predicted density. The transformation conditions for interconverting these polymorphs were as follows: A, loss of solvent at room temperature, heating at 340 K or mechanical grinding at room temperature; B, heating at 358–383 K. (b) Nitrogen isotherms (77 K); (c) methane isotherms (115 K); filled circles, adsorption experiments; unfilled circles, desorption experiments; filled triangles, adsorption simulations. Reprinted with permission.[53] Copyright 2017 Nature Publishing Group.

These studies indicate the potential to further increase gas storage and working capacities of HOF materials through the design of isoreticular framework. Overall, further endeavors for highly porous structure will facilitate eventual implementation of some promising HOFs for energy gas storage in the near future.

3.2 Carbon dioxide capture

The removal of carbon dioxide is heavily involved during many processes owing to significant environmental, energy and health concerns. For example, natural gas upgrading, flue gas treatment and CO_2 concentration control in closed air spaces. In particular, the removal of acidic gaseous components including CO_2 is an industrial scale process in natural gas industry. Because the presence of CO_2 will not only lower the energy level of natural gas but also corrode the pipeline. Natural gas is an important energy source owing to its abundant reserves and high energy intensity, giving a worldwide gas consumption of over 3.5 trillion cubic meters in 2015. A variety of CO_2 in different gas sources, ranging from casing-head gas, shale gas, and biogas to coal-bed methane, are often removed by amine scrubbing, while the corresponding regeneration is corrosive and energy-intensive. In contrast, CO_2 removal at ambient temperature based on physically adsorptive porous materials is a very promising approach for related processes. As emerging porous materials, HOFs have exhibited high capture capacity and selectivity for CO_2/CH_4 mixture.

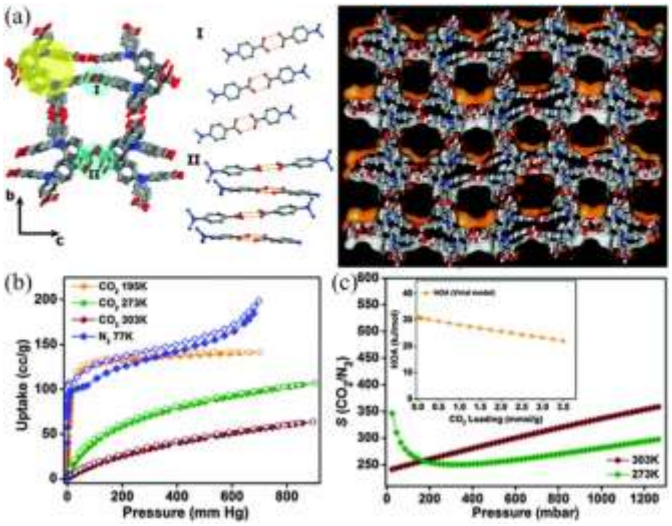

Fig. 10 (a) The crystal structure of IISERP-HOF1 with 1D channels. (b) N_2 and CO_2 isotherms of IISERP-HOF1. (c) The IAST plots of IISERP-HOF1 for 15:85 CO_2/N_2 mixture. The inset shows the HOA plot calculated using virial methods. Reproduced with permission.[121] Copyright 2016, Royal Society of Chemistry.

Certain interpenetration is beneficial for the structure rigidity of HOFs. To control the degree of interpenetration, Vaidhyanathan *et al*. utilized 4,4',4''-nitrilotribenzoic acid (H_3NTB) with a near-propeller shape to construct a 3D permanently porous HOF ($C_{21}H_{15}NO_6$) (IISERP-HOF1,[121] also HOF-11[123]) with 11-fold interpenetrated networks of 3-connected **ths** topology. Each carboxylic acid group of H_3NTB forms dimeric synthon with another one via strong intermolecular H-bonding (O–H···O 2.58–2.64 Å). This HOF contains 1D cylindrical channels with aperture size of 6.2 × 6.8 $Å^2$ (Fig. 10). The solvent-accessible void of this HOF is ~33% of the total cell volume. This HOF can retain its crystallinity until about 553 K. Depending on the activation conditions or synthesis methods, the experimental BET surface area of this HOF ranges from 412 $m^2\ g^{-1}$ to 687 $m^2\ g^{-1}$. This HOF shows high CO_2 uptake capacity of 4.8 and 2.9 mmol g^{-1} at 273 and 303 K, respectively, resulting in high CO_2/N_2 selectivity of 350 at 303 K. Notably, this HOF was synthesized by solvothermal method, involving crystallization in acetic acid at 423 K. And, this HOF exhibits remarkable stability towards acid and water. Solvent diffusion of hexane into the tetrahydrofuran solution of this tricarboxylic acid gave the same structure, HOF-11. The single-crystal structure of desolvated HOF-11 can be successfully obtained after mild activation, demonstrating its framework robustness that originated from interpenetration.

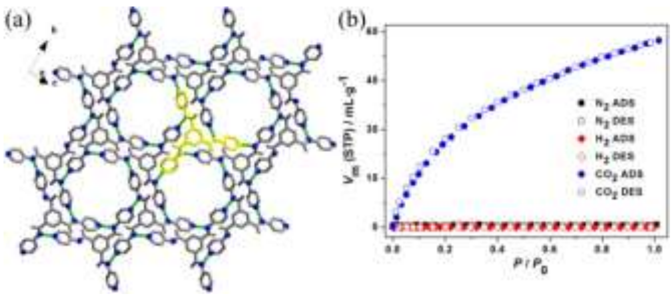

Fig. 11 (a) Crystal structure of HOF-8, showing 2D supermolecular layer. (b) N_2, H_2, and CO_2 sorption isotherms for HOF-8d at 298 K. Reprinted with permission.[91] Copyright 2013 American Chemical Society.

Another relatively stable HOF $(C_{24}H_{18}N_6O_3)\cdot0.15DMF\cdot3H_2O$ (HOF-8) is assembled from a tri-pyridine ligand N^1,N^3,N^5-tris(pyridin-4-yl)benzene-1,3,5-tricarboxamide (TPBTC) that integrates amide and pyridyl groups to serve as H-bonding donors and acceptors.[91] Each tri-pyridine ligand contains 6 H-bonding sites to connect with three other ligands via multiple intermolecular H-bonding (N–H···N 2.96-3.02 Å), giving a 2D honeycomb layered structure (Fig. 11), which is further stacked through interlayer π···π interactions. This HOF contains 1D channels with cavity size of 4.5 × 6.8 $Å^2$. The solvent-accessible void of this HOF is estimated to ~24%. This HOF exhibits excellent stability upon water and certain organic solvent (benzene and hexane). Variable-temperature PXRD and thermogravimetric analysis demonstrated the good thermal stability of this HOF. The activation of its partially deuterated structure HOF-8d enables this HOF to show permanent porosity and selective adsorption toward CO_2 over N_2 and H_2. The uptake capacity of HOF-8d for CO_2 at 298 K and 1 atm is 57.3 cm^3 (STP) g^{-1}, which is far higher than those negligible ones for N_2 and H_2. In addition, this HOF also shows selective adsorption of benzene over *n*-hexane, cyclohexane, toluene, or *p*-xylene.

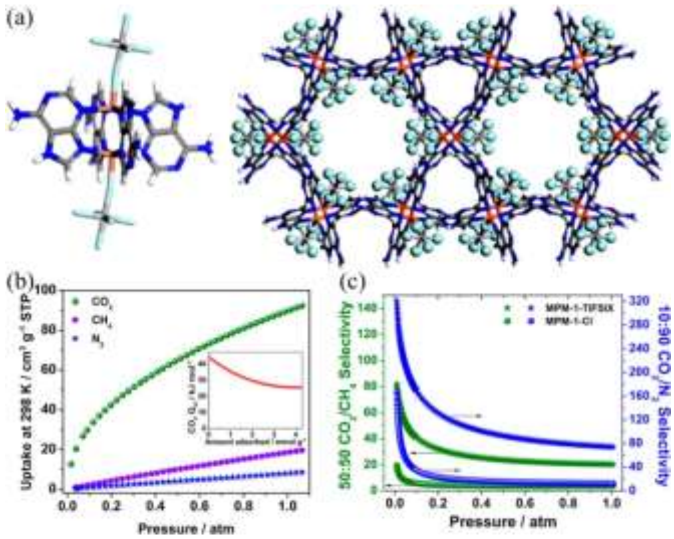

Fig. 12 (a) Views of the paddle-wheel complexes and the assembled networks along the crystallographic [001] axis in MPM-1-TIFSIX. (b) Low-pressure CO_2, CH_4, and N_2 isotherms collected at 298 K and (inset) CO_2 Q_{st} for MPM-1-TIFSIX. (c) IAST selectivities for 50:50 CO_2/CH_4 (green; left ordinate) and 10:90 CO_2/N_2 (blue; right ordinate) binary mixtures predicted at 298 K for MPM-1-TIFSIX. Reprinted with permission.[124] Copyright 2013 American Chemical Society.

Using metal complexes as H-bonding units for the construction of HOFs is expected to largely extend the diversity of this type of porous materials.[125-129] Based on a discrete dinuclear copper complex, Zaworotko *et al*. reported a robust HOF $[Cu_2(ade)_4(TiF_6)_2]\cdot 2CH_3CN$ (MPM-1-TIFSIX, ade = adenine) synthesized from solvent diffusion, showing high CO_2 uptake capacity and selectivity under ambient conditions (Fig. 12).[124] In this HOF, each paddle-wheel copper complex interacts with eight adjacent molecules via N–H···N (2.99 Å) and N–H···F (2.73–2.94 Å) interactions. This HOF contains hourglass shaped channels with diameter of about 7.0 Å, featuring solvent-accessible volume of 49.4%. The experimental BET surface area of this HOF is 840 m^2 g^{-1} calculated from the CO_2 sorption isotherm at 195 K. At 298 K and 1 atm, this HOF shows high CO_2 uptake capacity (89.6 cm^3 g^{-1}) that is superior to those for CH_4 (18.5 cm^3 g^{-1}) and N_2 (8.0 cm^3 g^{-1}), resulting in high adsorption selectivities for 10/90 CO_2/N_2 (74.1) and 50/50 CO_2/CH_4 (20.3), which can be attributed to its high affinity toward CO_2 at low loading (44.4 kJ mol^{-1}). In addition, MPM-1-TIFSIX shows certain thermal stability and water stability.

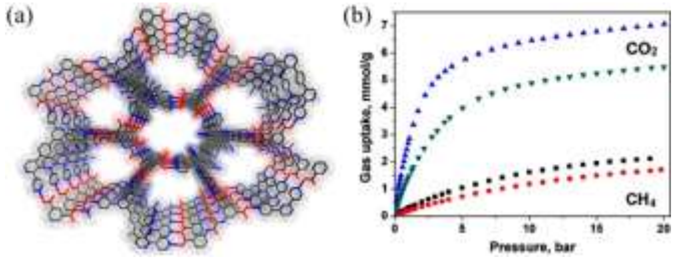

Fig. 13 (a) The 3D porous structure of SOF-7 with 1D channels viewed from crystallographic [100] axis. (b) CO_2 and CH_4 isotherms for SOF-7a at 273 K and 298 K in the pressure range 0–20 bar. Reprinted with permission.[107] Copyright 2014 American Chemical Society.

In terms of constructing new HOFs, mixed-ligands is a very promising strategy based on the known ligands without further design of new ligands. Schröder et al. reported a robust binary HOF (SOF-7) by incorporating the complementary pyridyl and carboxyl groups from independent ligands, which shows high CO_2 adsorption and selectivity (Fig. 13).[107] In SOF-7, $(C_{40}H_{20}N_{10})(C_{18}H_{12}N_2O_{10})\cdot 7DMF$, each carboxylic acid (5,5′-bis-(azanediyl)-oxalyldiisophthalic acid) connects with four adjacent pyridine ligands (1,4-bis-(4-(3,5-dicyano-2,6-dipyridyl)pyridyl)benzene) via multiple O–H···N (~2.60 Å) interactions, giving a 3D network of four-fold interpenetrating **cds** topology. After guest removal, the solvent-accessible void space was estimated to be 48% for SOF-7. This HOF contains 1D pore channels with aperture size of 13.5 × 14.0 Å^2, featuring cyano and amide groups on the pore surface for potential guest binding. This HOF shows good thermal stability and chemical stability. The BET surface area of SOF-7a was estimated to be 900 m^2 g^{-1} based on the CO_2 adsorption isotherm at 195 K. At 1 bar and 298 K, the CO_2 uptake capacity of SOF-7a is 6.53 wt % (1.49 mmol g^{-1}), further increasing to 24.1 wt % (5.48 mmol g^{-1}) at 20 bar, which is superior to those of 0.35 wt % (0.22 mmol g^{-1}) and 2.74 wt % (1.71 mmol g^{-1}) for CH_4. Based on Henry's Law constants, the CO_2/CH_4 selectivity was estimated to be 9.1 at 298 K and 1 bar. The adsorption heat for CO_2 is calculated to be 21.6 kJ mol^{-1}. The amide and cyano groups on the pore surface are supposed to account for such selective separation as revealed by modeling studies.

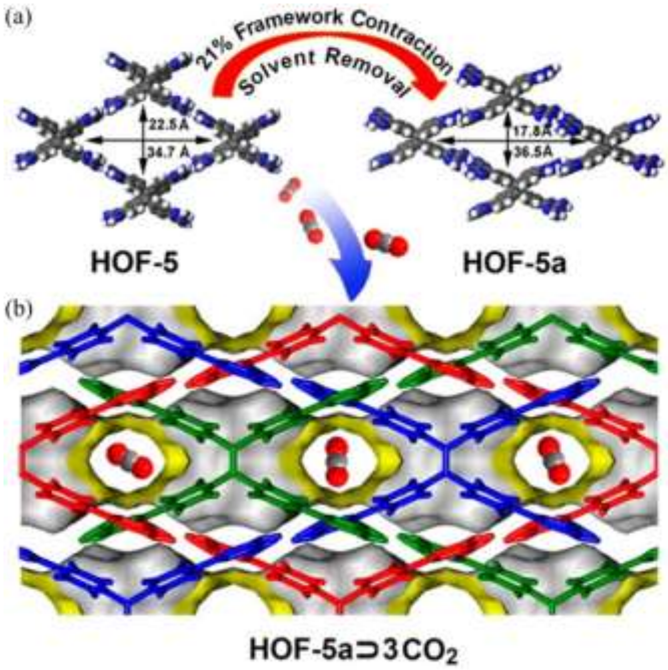

Fig. 14 (a) Schematic diagram about structural transformation from HOF-5 to HOF-5a and (b) CO_2 sorption in pore structure of HOF-5a. Reprinted with permission.[130] Copyright 2015 American Chemical Society.

Compared to other pure organic porous materials, the crystallinity and permanent porosity of HOFs enable certain technologies for crystallographic diffraction to be applicable for the determination of adsorption locates. In 2015, we reported a flexible microporous HOF ($C_{38}H_{32}N_{20}$, HOF-5) that showing reversible structure transformation during solvent removal, exhibits high CO_2 adsorption capacity (Fig. 14).[130] The

DAT-based (DAT = 2,4-diamino-1,3,5-triazine) ligand 4,4′,4′′,4′′′-tetra(2,4-diamino-1,3,5-triazin-6-yl)tetraphenylethene connects with eight adjacent ligands via multiple N–H···N (2.92–3.38 Å) interactions, giving a 3D network of binodal (4,6)-connected topology. HOF-5 contains 2D intersected channels with aperture sizes of ~3.9 × 5.4 and ~4.0 × 6.8 $Å^2$, in which the solvent-accessible void is 55.3%. Desolvation of acetone-exchanged sample gave guest-free HOF-5a, accompanying by a contraction of ~21% in unit cell volume, as revealed by structural refinement from its PXRD pattern. More and strengthened N–H···N (2.92–3.01 Å) interactions can be observed in HOF-5a. After guest removal, the solvent-accessible void space reduced to 41.1% in HOF-5a. The N_2 sorption isotherm of HOF-5a at 77 K exhibits a stepwise shape with a hysteresis, giving a pore volume of 0.44 $cm^3\ g^{-1}$ (P/P_0 = 0.13) that is consistent with that of HOF-5a, and a total pore volume of 0.55 $cm^3\ g^{-1}$ (P/P_0 = 0.96). The BET surface area of HOF-5a was estimated to be 1101 $m^2\ g^{-1}$. The uptake capacity of HOF-5a for CO_2 under ambient condition is up to 117.1 and 90.0 $cm^3\ g^{-1}$ (at 273 and 296 K, respectively), which represents the benchmark of HOFs for CO_2 capture under mild condition. The adsorption enthalpy of HOF-5a is 22.8 kJ mol^{-1} for CO_2. In contrast, HOF-5a shows much lower uptake capacity for CH_4 (32.0 $cm^3\ g^{-1}$) and N_2 (8.2 $cm^3\ g^{-1}$) at 296 K and 1 atm, giving high adsorption selectivities for 10/90 CO_2/N_2 (22.4) and 50/50 CO_2/CH_4 (5.0). The adsorption locates of CO_2 in this HOF was successfully observed from the powder neutron diffraction data of HOF-5a·1.5CO_2, showing high packing density of CO_2 array. In addition, this HOF also exhibits unique sorption response upon C_2H_2 with high uptake capacity.

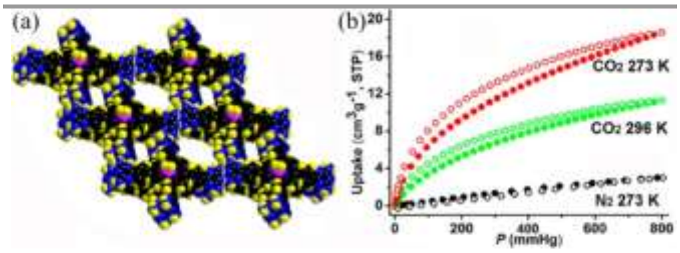

Fig. 15 (a) The 3D porous structure of HOF-7 viewed from crystallographic [100] axis. (b) Gas sorption isotherms of HOF-7a (solid symbols: adsorption; open symbols: desorption). Reprinted with permission.[131] Copyright 2015 American Chemical Society.

Another well-known functional moiety, porphyrin, was also employed to construct porous HOFs for CO_2 capture. For example, the self-assembly of zinc 5,10,15,20-tetrakis(4-(2,4-diaminotriazinyl)phenyl)porphyrin (ZnTDPP, $C_{56}H_{42}N_{24}Zn$) via solvent diffusion gave HOF-7 with 2D double-layered structure.[131] In such layered structure, each ZnTDPP in HOF-7 forms multiple N–H···N (2.92–3.06 Å) and O–H···N (2.88 Å) interactions with five different ZnTDPP molecules using their DAT moieties and coordinated water molecule. HOF-7 contains 3D intersected pore channels with pore size of 3.2 × 4.7 and 4.2 × 6.7 $Å^2$. The BET surface area of activated HOF-7a is only 124 $m^2\ g^{-1}$ calculated from the CO_2 sorption isotherm at 195 K. HOF-7a exhibits high adsorption selectivity for 15/85 CO_2/N_2 (40) at 273 K and 1 atm (Fig. 15).

Ultramicroporous HOFs are also explored for CO_2 separation. A transformed HOF ($C_{18}H_{21}N_{15}$), HOF-9a,[132] showing a binodal (3,9)-connected topology with 1D cylindrical channels (~3.4 × 6.8 $Å^2$, void: ~22%, BET: 286 $m^2\ g^{-1}$), can selectively adsorbs CO_2 over CH_4 and N_2 with an uptake capacity of 40 $cm^3\ g^{-1}$ under ambient condition.

The aforementioned examples have demonstrated HOFs can serve as promising CO_2 sorbents like other porous media. Importantly, the control of pore structure in HOF materials can be achieved by means of the design of organic moieties, facilitating the development of this class of materials as novel porous materials for adsorptive applications.

3.3 Hydrocarbons separation

The separation of hydrocarbon mixtures is very important, challenging and energy-intensive process in the petrochemical industry. Among various hydrocarbons, the light hydrocarbons including methane, ethylene, ethane, acetylene, propylene and propane take the most important part. However, the separation of these gases of low boiling points through cryogenic distillation requires tremendous energy consumption. Adsorptive separation technologies thus have been proposed as alternative technologies for potential energy saving. The high porosity of HOFs enables them to show high gas uptake. But high selectivity is another important aspect, which requires strong binding sites. It should be noted that the flexibility and solution processability set HOFs apart from other polymeric porous framework, which provides new possibilities toward further membrane fabrication for advanced gas separation and purification.

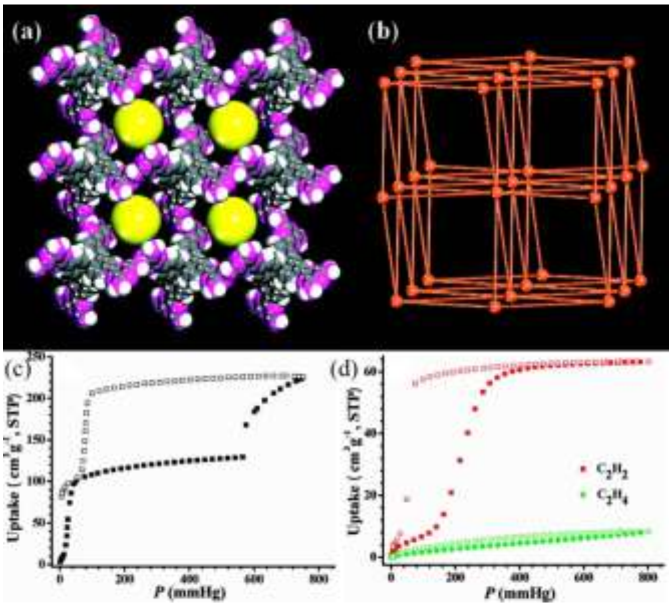

Fig. 16 (a) The X-ray crystal structure of HOF-1 showing 1D channels along crystallographic [001] axis. (b) The **bcu** network topology of HOF-1. (c) CO_2 sorption isotherm at 196 K and (b) C_2H_2 and C_2H_4 sorption isotherms at 273 K. Reprinted with permission.[28] Copyright 2011 American Chemical Society.

Although the establishment of HOFs with permanent porosity was not realized until 2010, their potential in the realm of hydrocarbons separation/purification has been proven almost at the same time as those of MOFs. In 2011, we reported the first microporous HOF for selective C_2H_2/C_2H_4 separation under ambient condition (Fig. 16).[28] In this studied

HOF, each ligand 4,4',4'',4'''-tetra(4,6-diamino-*s*-triazin-2-yl)tetraphenylmethane connects with eight adjacent ligands via multiple N–H···N (3.03–3.08 Å) interactions, giving a 3D network of 8-connected **bcu** toology. HOF-1 contains 1D pore channels with cavity sizes of ~8.2 Å in diameter, in which the solvent-accessible void is 42%. Half of the amino groups in the ligand are accessible for guest binding, that are exposed on the pore surface. This HOF shows a certain degree of framework flexibility as indicated by the cell contraction after partial solvent removal reported by Wuest. HOF-1 lost all its guest molecules at 443 K, giving HOF-1a, which shows no weight loss until >693 K. The CO_2 sorption isotherm of HOF-1a at 195 K exhibits a stepwise shape with a hysteresis. The BET surface area of HOF-1a was estimated to be 359 m^2 g^{-1}. Owing to the framework flexibility, HOF-1a shows unique gate-opening sorption behavior at ambient conditions for C_2H_2. At 273 K, HOF-1a can take up C_2H_2 of 63.2 cm^3 g^{-1} (at 800 mmHg), while only 8.3 cm^3 g^{-1} for C_2H_4, giving a high C_2H_2/C_2H_4 uptake ratio of 7.6. The adsorption enthalpies of HOF-1a for C_2H_2 and C_2H_4 at zero coverage were estimated to be 58.1 and 31.9 kJ mol^{-1}, respectively. The strong binding affinity of HOF-1a for C_2H_2 results in a high Henry selectivity of 19.3 at 273 K.

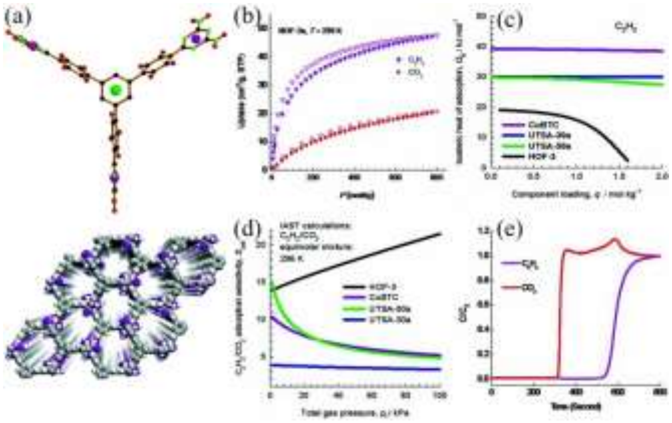

Fig. 17 (a) The X-ray crystal structure of HOF-3 in three-dimensional packing showing the 1D hexagonal channels of about 7.0 Å in diameter along crystallographic [001] axis. (b) Sorption isotherms of C_2H_2 and CO_2 of HOF-3a at 296 K. (c) comparison of the heats of adsorption of C_2H_2 in HOF-3a and various MOFs. (d) IAST adsorption selectivities of C_2H_2/CO_2 in equimolar mixture in HOF-3a and various MOFs at 296 K. (e) experimental column breakthrough curve for an equimolar C_2H_2/CO_2 mixture (296 K, 1 bar) in an adsorber bed packed with HOF-3a. Reproduced with permission.[133] Copyright 2015 Wiley-VCH.

The implementation of establishing permanent porosity initiated great research endeavours on HOFs for the challenging separation of important hydrocarbons. Another example of using HOFs for C_2H_2 purification was revealed by HOF-3, showing recorded-high selectivity of HOFs for C_2H_2/CO_2 separation (Fig. 17).[133] In this triangular ligand of C_3 symmetry, there are three DAT groups on the 1,3,5-Triphenylbenzene scaffold. Each ligand connects with six adjacent ligands via multiple N–H···N (2.90 and 3.11 Å) interactions, giving a 3D rod-packing network of **srs** toology. HOF-3 contains 3D pore channel with sizes of ~7.0 Å in diameter, in which the solvent-accessible void is about 75%. The BET surface area based on the CO_2 sorption isotherm of activated HOF-1a at 195 K was estimated to be 165 m^2 g^{-1}. HOF-3a shows selective adsorption of C_2H_2 (47 cm^3 g^{-1}) over CO_2 (21 cm^3 g^{-1}) at 296 K and 1 atm, giving high adsorption selectivity for 50/50 C_2H_2/CO_2 (21). Notably, for the first time, in this work, experimental column breakthrough was used to evaluate the separation performance of porous materials for C_2H_2/CO_2 mixture.

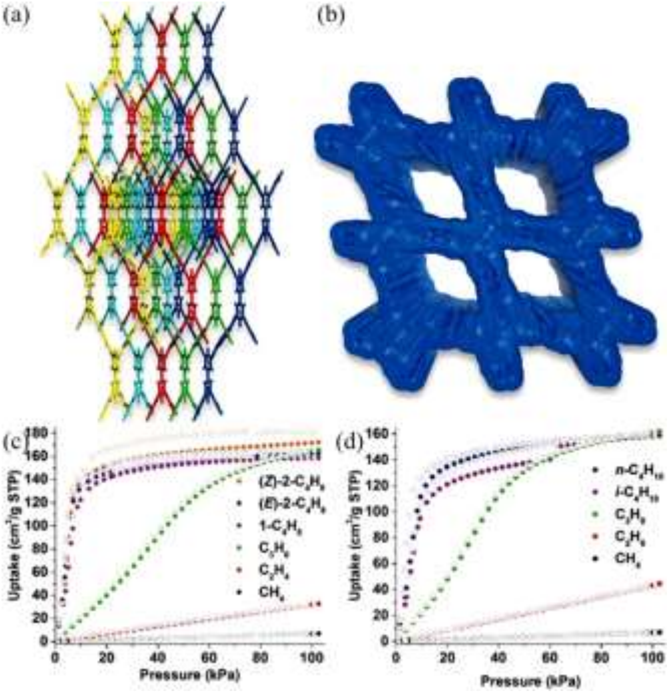

Fig. 18 (a) The X-ray crystal structure of HOF-TCBP showing a 5-fold interpenetrated **dia** framework. (b) Connolly representation of the 1D channels along crystallographic [100] axis. (b) Sorption isotherms of C_2H_2 and CO_2 of HOF-3a at 296 K. (c-d) The sorption isotherms of HOF-TCBP for the light hydrocarbons at 295 K. Reproduced with permission.[112] Copyright 2017 Wiley-VCH.

Stable and robust HOFs are highly favourable for the further development of this type of porous materials. In this context, Wu, Yuan and Hong et al. reported an ultrastable and robust HOF (HOF-TCBP, H_4TCBP = 3,3',5,5'-Tetrakis-(4-carboxyphenyl)-1,1'-biphenyl), showing selective separation of several light hydrocarbons over methane under ambient conditions (Fig. 18).[112] Each ligand connects with four adjacent ligands through four pairs of intermolecular -COOH···HOOC- hydrogen bonds, with strong O–H···O (2.62 Å) interactions, which further stack together via strong π···π interactions. These interactions jointly contribute to the high stability of HOF-TCBP. Considering the ligand of distorted tetrahedral configuration as a 4-connected node, HOF-TCBP can be simplified as five-fold interpenetrated **dia** topology, which contains 1D rhombic channel pore channels (17.8 × 26.3 $Å^2$). The solvent-accessible void was estimated 56%. Based on the N_2 sorption isotherm at 77 K, the BET surface area of this HOF was estimated to be 2066 m^2 g^{-1}, which is superior to those of most reported HOFs. HOF-TCBP shows excellent water stability as revealed by corresponding PXRD patterns and BET surface area of water-treated samples. Also, this HOF can retain most of its permanent porosity at high temperatures (about 473 K). Notably, the porosity of HOF-TCBP can be easily regenerated by simple recrystallization. This HOF shows selective adsorption of C_3 and C_4 (158-172 cm^3 g^{-1}) over CH_4 (7.4 cm^3 g^{-1}) at 295 K and 1 bar, giving high adsorption selectivity for 50/50

C_4/CH_4 (147–241), which is promising for the separation and purification of light hydrocarbons.

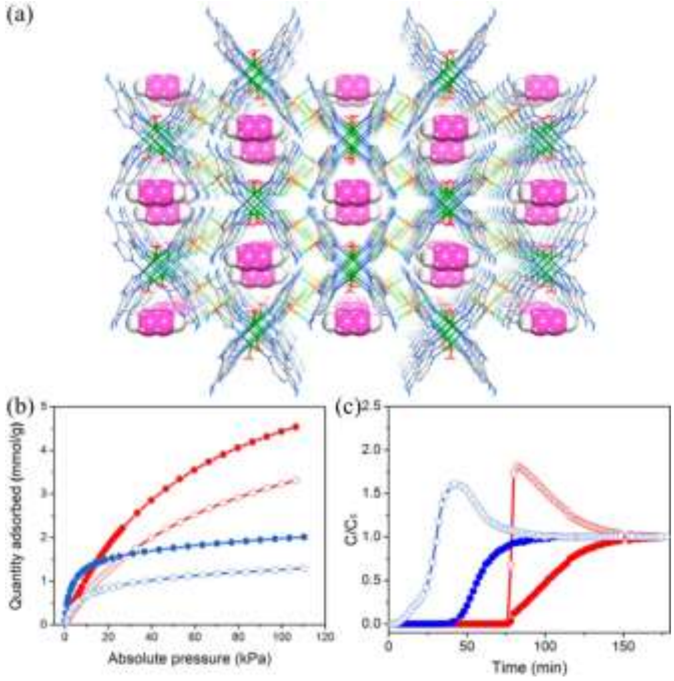

Fig. 19 (a) Neutron crystal structure of HOF-21a·C_2D_2 viewed along crystallographic [001] axis. (b) Adsorption isotherms of C_2H_2 (solid) and C_2H_4 (hollow) on HOF-21a (blue) and MPM-1-TIFSIX (red) at 298 K. (c) Experimental column breakthrough curves for 50:50 C_2H_2/C_2H_4 binary mixture at 298 K and 1 bar in an adsorber bed packed with HOF-21a (blue) or MPM-1-TIFSIX (red). Hollow dot is for C_2H_4, and solid dot is for C_2H_2. Reprinted with permission.[111] Copyright 2018 American Chemical Society.

HOFs can be extended to metal-complex based structures as long as their linkages of networks are through H-bonding. Incorporating metal-complexes with geometric rigidity into HOFs not only facilitates the retention of permanent porosity, but also introduces functional sites. Recently, a microporous hydrogen-bonded metal-complex framework $[Cu_2(ade)_4(H_2O)_2](SiF_6)_2$ (HOF-21) was realized for selective separation of C_2H_2/C_2H_4 at room temperature (Fig. 19).[111] In HOF-21, through H-bonding, each metal cluster $[Cu_2(ade)_4(H_2O)_2]^{4+}$ connects with two adjacent clusters and eight SiF_6^{2-} ions, while each free SiF_6^{2-} ion contacts with four metal clusters. There are three types of H-bonding interactions, including N–H···N (3.06 Å), N–H···F (2.75–3.04 Å) and O–H···F (2.89–2.91 Å) interactions. HOF-21 contains 1D pore channels with aperture sizes of ~3.6 Å in diameter. The BET surface area of HOF-21a was estimated to be 339 $m^2\ g^{-1}$ based on the CO_2 sorption isotherm at 195 K. At 298 K and 1 bar, HOF-21a can take up C_2H_2 of 1.98 mmol g^{-1}, while 1.27 mmol g^{-1} for C_2H_4, giving a C_2H_2/C_2H_4 IAST selectivity of 7.1. Such selective sorption of C_2H_2 over C_2H_4 was attributed to the strong C–H···F interactions between acetylene molecules and SiF_6^{2-} binding sites, which is validated by the binding energy of C_2H_2 and its adsorption locates from neutron powder diffraction studies. Column breakthrough experiments demonstrated that C_2H_2 can be successfully removed from C_2H_4 by using HOF-21a. This HOF also shows considerable water stability and easy healing.

In certain framework geometry, the existing of intrinsic pore space might be possible but usually would be minimized by accompanied interpenetrations, which can in turn stabilize the framework. Zentner and Lai *et al.* reported several HOFs from 1,3,5-Tris(4-carboxyphenyl)benzene and its derivatives, showing high and robust porosity after multiple interpenetrations.[134,135] Recently, Bae and Kim have demonstrated such HOFs can be applied in separation of light hydrocarbons.[136] To be specific, HOF-BTB based on 4,4′,4′′-benzene-1,3,5-triyl-tris(benzoic acid) was studied for selective adsorption of C_2H_2, C_2H_4 and C_2H_6 over CH_4, which contains eight-fold interpenetration of 2D hexagonal sheets. Based on the N_2 sorption isotherm at 77 K, the BET surface area of this HOF was estimated to be 955 $m^2\ g^{-1}$, with measured pore size of 12–16.6 Å. At 295 K and 1 bar, this HOF takes up C_2H_2 of 2.87 mmol g^{-1}, C_2H_4 of 2.48 mmol g^{-1}, and C_2H_6 of 3.09 mmol g^{-1}, which gives a C_2H_6/CH_4 (50:50) IAST selectivity of 14.

Indeed, HOFs can be applied as porous adsorbents for hydrocarbon separation, showing high uptake capacity and considerable selectivity. In terms of separating gas molecules of small dipole and/or quadrupole moments, strong binding sites often dominate. Hence, to improve separation performance, the introduction of strong binding sites should be taken into account for future design of HOF materials.

3.4 Other volatile adsorbates

Besides the carbon dioxide capture and hydrocarbon separation, there are also few examples about HOFs for other gas separation, including fluorocarbons over nitrogen and air separation. In fact, the capture of harmful volatile gas/vapour for environmental concern is an important application of porous materials, in which HOFs still in its early stage. Therefore, there are great potential for HOF materials to capture volatile gaseous molecules.

Miljanić and co-workers reported a stable HOF for the adsorption of fluorocarbons (FCs) and chlorofluorocarbons (CFCs), which is constructed from a fluorinated trispyrazole ligand ($C_{33}H_{12}F_{12}N_6$, Fig. 20).[88] In this HOF, each organic ligand connects to six adjacent ligands via pyrazole trimer units with multiple N–H···N (2.78–2.87 Å) interactions, giving 2D honeycomb-like lattices of **hnb** topology, which further stack together via strong π···π interactions with centroid–centroid distances of 3.42–3.69 Å. This HOF contains 1D hexagonal pore channels (16.5 Å) with a solvent-accessible void ratio of 56%. As demonstrated by PXRD analysis, this HOF exhibits remarkable chemical stability to many organic solvents, water and acid/base aqueous solutions, and high thermal stability upon exposure at >523 K. The BET surface area of this HOF was determined to be 1159 $m^2\ g^{-1}$ based on the N_2 sorption isotherm at 77 K. This HOF takes up a negligible amount of H_2O vapour owing to its hydrophobicity, but can favorably capture large amounts of FCs and CFCs, including chloroform, dichloromethane, CCl_2FCClF_2 (CFC-113), and $CF_3CF_2CHCl_2$ (HCFC-225ca). In particular, this HOF adsorbs large amounts of perfluorohexane (74 wt%) at room temperature with good reversibility and fast adsorption dynamic. Later, in their follow-up work,[103] several isostructural HOFs extended from this prototypal HOF were successfully obtained by increasing length of the linker, showing tunable porosity.

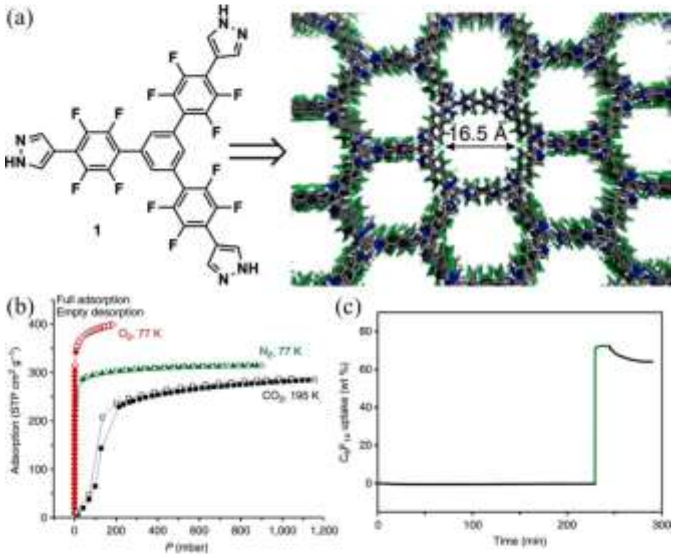

Fig. 20 (a) The X-ray crystal structure of fluorinated trispyrazole showing a hexagonal network results, with infinite fluorine-lined channels protruding throughout the structure along crystallographic [001] axis. (b) Gas sorption isotherms for N_2, O_2 and CO_2. (c) Uptake of perfluorohexane as the function of time, upon to the flow of C_6F_{14}-enriched nitrogen. Reprinted with permission.[88] Copyright 2014 Nature Publishing Group.

Zhang et al. reported a 3D highly-symmetric HOF, $(C_{12}H_3F_9N_6)\cdot 1/6C_{12}H_3F_9N_6$, that showing selectively adsorbs O_2 over Ar and N_2 (Fig. 21).[137] This HOF is constructed based on trifluoromethyl substituted benzotrisimidazole, which connects with three adjacent organic ligands through three pairs of N–H···N (3.01 Å) interactions in this framework. This HOF can undergo a water-induced reversible crystal-to-crystal transformation. This HOF shows a 3-connected srs topology, containing 3D intersected channels (void ratio of 21.7%) with aperture size of 4.6 × 2.9 Å^2. The BET surface area of this HOF was estimated to be 131 m^2 g^{-1} based on the CO_2 sorption isotherm at 195 K. At 77 K, this HOF can take up O_2 of 50 cm^3 g^{-1}, while shows negligible capacity for Ar and N_2 (3.3 and 4.8 cm^3 g^{-1}, respectively), giving a Henry's law selectivity of 119 and 59 for O_2/Ar and O_2/N_2, respectively. In addition, by changing the size of the substituent group, another 2D HOF with honeycomb-like network can be obtained.

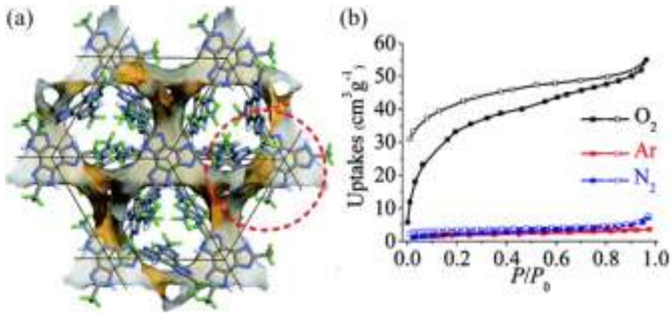

Fig. 21 (a) The 3D channel (orange/gray surfaces) defined by the hydrogen-bonded network and (b) the O_2/Ar/N_2 sorption isotherms at 77 K for trifluoromethyl benzotrisimidazole. Curves with solid symbols represent adsoprtion isotherms, while desopriton isotherms are with open symbols. Reproduced with permission.[137] Copyright 2016, Royal Society of Chemistry.

As presented above, HOFs are very promising porous materials for various challenging gas storage and separation. The implementation of permanent porosity enables HOFs to serve as novel porous materials for gas sorption, which is particularly important in advancing the HOF chemistry. Despite the retention of porosity during the removal of guest molecules is challenging, many HOFs constructed from different H-bonding units can still show remarkable thermal stability, solvent stability and even water stability, which affords good modeled structure for further development of permanently porous HOFs. Continuous endeavours on exploring porous HOFs are expected, as stimulated by the aforementioned achievements on realizing HOF materials for various gas separations.

4. HOFs for molecular recognition

Molecular recognition plays an important role in biological systems, involving specific intermolecular interactions through noncovalent binding including H-bonding, $\pi\cdots\pi$ interactions and van der Waals forces. The implementation of establishing permanent porosity renders HOFs as a good platform to understand similar recognition processes. In specific, the following features are particularly important: i) the immobilization of functional sites into porous framework can improve specific recognition; ii) the relatively flexible and adaptive framework that facilitates potential host-guest collaborative interactions; iii) the high crystallinity that provides the possibility to visualize the host-guest interactions via powerful crystallographic tools. For instance, the introduction of chiral center affords asymmetric pore environment for enantioselective separation, while extra H-bonding donors/acceptors offer binding sites for complement analytes.

In 2014, we reported the first example of a chiral HOF based on a 1,1'-bi-2-naphthol (BINOL) derivative, (*R*)-4,4',6,6'-tetra-(2,4-diamino-1,3,5-triazin-6-yl)-2,2'-diethoxy-1,1'-binaphthalene, ($C_{36}H_{34}N_{20}O_2$, HOF-2, Fig. 22).[138] This new organic ligand is exclusively designed by covalently incorporated the DAT H-bonding units onto the (*R*)-BINOL scaffold. In this homochiral HOF, each organic ligand connects to six adjacent ligands via DAT dimers with multiple N–H···N (2.98–3.34 Å) interactions, giving 3D uninodal 6-connected network. This HOF contains 3D intersected pore channels (pore size: 4.8 Å) with chiral centers exposing on the pore surface, which facilitates the enantioselective recognition of small molecules. The solvent-accessible void ratio of this HOF was estimated to be 54.3%. The BET surface area of HOF-2a was determined to be 238 m^2 g^{-1} based on the CO_2 sorption isotherm at 195 K. Utilizing this homochiral HOF, we realized enantioselective separation of racemic secondary alcohols for the first time. Interestingly, this HOF shows higher enantioselectivity for aromatic secondary alcohols than that for aliphatic secondary alcohols. In particular, the enantiomeric excess (*e.e.*) value for 1-phenylethanol (1-PEA) in this HOF is up to 92%, as determined by HPLC. Single-crystal X-ray diffraction of 1-PEA included samples were applied to gain in-depth insight into the origin of high enantioselectivity. It is because *R*-1-PEA molecules form strong H-bonding (O–H···O 2.58 Å) with the diethoxy groups of the BINOL scaffold, while *S*-1-PEA molecules show weaker C–H···O (3.28–3.57 Å) interactions with the framework. In addition, the permanent porosity of this HOF can also realize gas storage/separation as revealed by its C_2H_2 adsorption at 273 K. Overall, this work represents the first example of homochiral porous HOFs for the enantioselective separation of small molecules as another critical potential application.

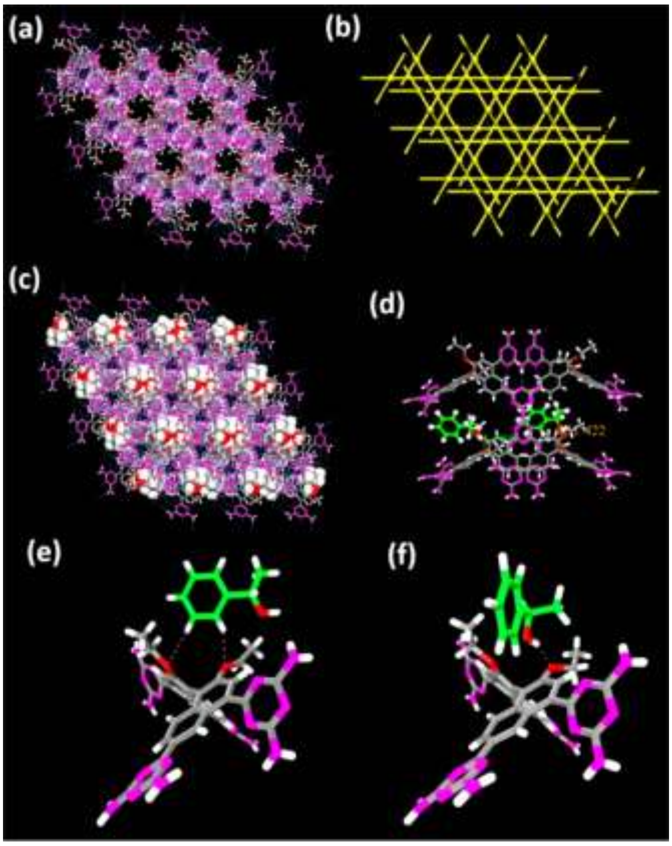

Fig. 22 X-ray crystal structure of HOF-2 featuring (a) three-dimensional hydrogen-bonded organic framework exhibiting 1D hexagonal pores along crystallographic [001] axis and (b) the uninodal 6-connected network topology. X-ray crystal structure of HOF-2⊃*R*-1-PEA indicating (c) the enantiopure *R*-1-PEA molecules residing in the channels of the framework along crystallographic [001] axis and (d) the chiral cavities of the framework for the specific recognition of *R*-1-PEA. Comparison of X-ray crystal structures of (e) HOF-2⊃*S*-1-PEA and (f) HOF-2⊃*R*-1-PEA. Reprinted with permission.[138] Copyright 2014 American Chemical Society.

Introducing functional sites into porous materials like MOFs is well recognized as efficient approach for the selective recognition of small molecules. But it is challenging to reserve similar sites during the assembly of HOFs. Recently, we reported a DAT-derived HOF (TDTTB)·$(H_2O)_2$·3DMSO (HOF-9, TDTTB = 1,3,5-tris(2,4-diamino-1,3,5-triazin-6-yl)-2,4,6-trimethyl-benzene) containing unbonded amine groups (Fig. 23), which exhibits highly selective recognition for pyridine (Py) over BTX aromatic compounds (BTX refers to benzene, toluene, and *o*-, *m*-, *p*-xylene).[132] This HOF is constructed from TDTTB dimers, which further connects with six other dimers through multiple N–H···N (2.94–3.47 Å) interactions, giving a 3D open framework of **pcu** topology. There are H_2O molecules located between TDTTB dimers that can further stabilize the framework through O–H···N (2.80–2.89 Å) and N–H···O (2.86–3.07 Å) interactions. HOF-9 contains 1D pore channels (6.9 × 8.8 $Å^2$) along crystallographic [100] axis, with free amino groups exposing on the pore surface, which facilitates the selective recognition of Py molecules. Simple adsorption studies under ambient condition demonstrated HOF-9 can take up 1 Py molecule per formula while no BTX molecules, as shown by corresponding NMR spectra. Single-Crystal structural analysis of HOF-9·2Py revealed that strong N–H···N (3.20 Å) interactions form between unbonded amino groups and Py molecules. The binding energy of Py in HOF-9 was calculated to be ~67 kJ mol^{-1}, which higher than that of benzene (~41 kJ mol^{-1}). Further selective adsorptions of Py from different binary equimolar mixtures confirm that the efficient recognition of Py from BTX aromatic molecules.

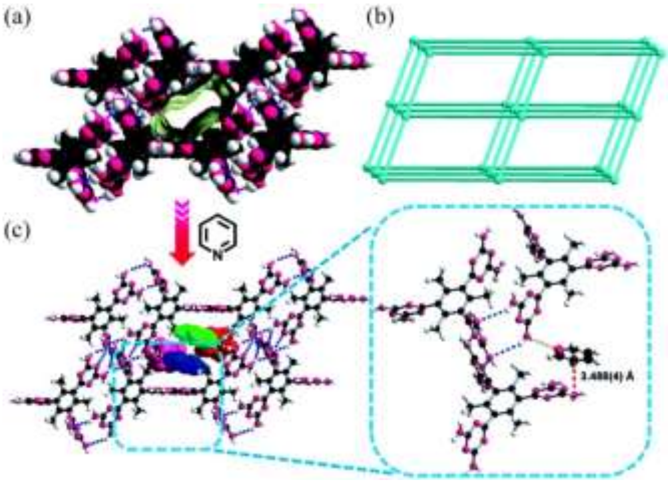

Fig. 23 Packing diagram of HOF-9 along the crystallographic [100] axis showing the pore surfaces of 1D channels highlighted as yellow/grey (inner/outer) curved planes; (d) a uninodal 6-connected *α*-Po net. (e) The crystal structure of HOF-9⊃Py indicating the hydrogen-bonding interactions between Py and the HOF-9 framework (yellow dashed line), the π–π interaction between the DAT group and Py molecule (red dashed line) and packed Py molecules residing in the channel of the framework along the crystallographic [100] axis. Reproduced with permission.[132] Copyright 2017, Royal Society of Chemistry.

To maximize the accessible surface of aromatic rings, Li *et al.* employed a rigid and non-coplanar triptycene derivative to construct HOF, showing selective adsorption for aromatic compounds and high efficient enrichment for fullerene molecule (Fig. 24).[139] This HOF is based on a imidazole ligand, 2,6,12-trihydrotripty[2,3-*d*:6,7-*d′*:12,13-*d″*]triimidazole (H_3TBI), which connects with six adjacent H_3TBI ligands through six N–H···N (2.80 Å, 170.4°) interactions, giving a 3D open framework (H_3TBI)·3DEF (FDM-15). This HOF contains hexagonal honeycomb-like channels with aperture sizes of ~11.5 Å in diameter. With very low density of 0.436 g cm^{-3}, this HOF exhibits permanent porosity with a BET surface area of 749 m^2 g^{-1}. Given the suitable pore size and desirable pore surface featuring aromatic rings, this HOF was applied to enrich fullerene (C_{60}, 10.5 Å in diameter) from toluene solution. The adsorbed C_{60} in this HOF is up to ~12 wt% of the final solid, giving a concentration of 420 times higher than that of original C_{60} solution. In addition, simple adsorption studies under ambient condition demonstrated this HOF can take up 1.3 *p*-xylene molecules per H_3TBI molecule while 0.74 molecule for toluene, as examined by corresponding NMR spectra. Further selective adsorptions of *p*-xylene from different binary equimolar mixtures confirm that the selective adsorption of *p*-xylene over toluene, *o*-xylene and ethylbenzene.

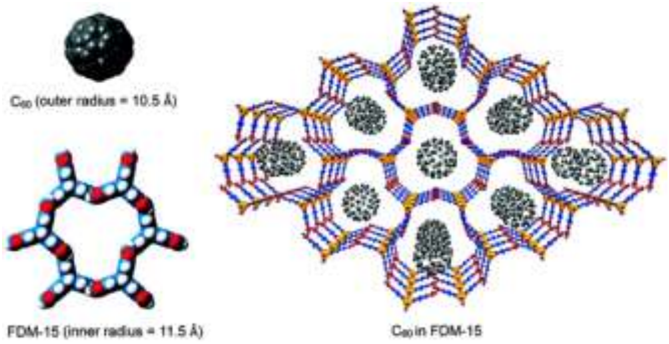

Fig. 24 Illustration of fullerene molecules distributed in the channels of FDM-15. Reproduced with permission.[139] Copyright 2017, Royal Society of Chemistry.

The flexibility of HOFs enables them to show adaptive framework transformation during different guest inclusion, which allows the retention of single crystallinity, facilitating direct visualization of corresponding host-guest interactions via single crystal X-ray diffraction. Ward et al. reported interesting guest discrimination from different pore channels based on single crystal analyses of various guest inclusion compounds of a guanidinium–sulfonate HOF (Fig. 25), guanidinium 1,2,4,5-Tetra(4-sulfonatophenyl)benzene (G_4TSPB).[140-142] In these compounds, each $TSPB^{4-}$ connects with 16 adjacent guanidinium cations using all its oxygen atoms through charge assisted N–H···O (2.6–3.1 Å) interactions, while each guanidinium cation connects with four $TSPB^{4-}$, giving 3D HOFs with 1D infinite H-bonding cylinders. This HOF contains three types of 1D channels, with cross-section areas of 18, 39 and 52 $Å^2$, respectively. This HOF can retain its single crystallinity upon the exchange of various solvents, owing to its sufficient framwork flexibility. Reversible guest exchange between inclusion compounds for dioxane ($C_4H_8O_2$), tetrahydofuran (C_4H_8O), and toluene (C_7H_8) gives single crystals of $(G_4TSPB)\cdot 5C_4H_8O_2$, $(G_4TSPB)\cdot 5C_4H_8O$, $(G_4TSPB)\cdot 3C_7H_8\cdot C_4H_8O_2$ and $(G_4TSPB)\cdot 3C_7H_8\cdot 0.5C_4H_8O$, respectively. For dioxane and tetrahydofuran molecules, they can take up all the three pore channels. But the toluene molecules show only partial guest exchange toward inclusion compounds of dioxane and tetrahydofuran, because the smallest pore channel is inaccessible for the larger toluene molecule. All three pore channels exhibit certain expansion and shrinkage after these solvent exchange processes. Notably, the related solvent exchange processes within this HOF are all single crystal to single crystal transformations, which is rarely reported for HOFs.

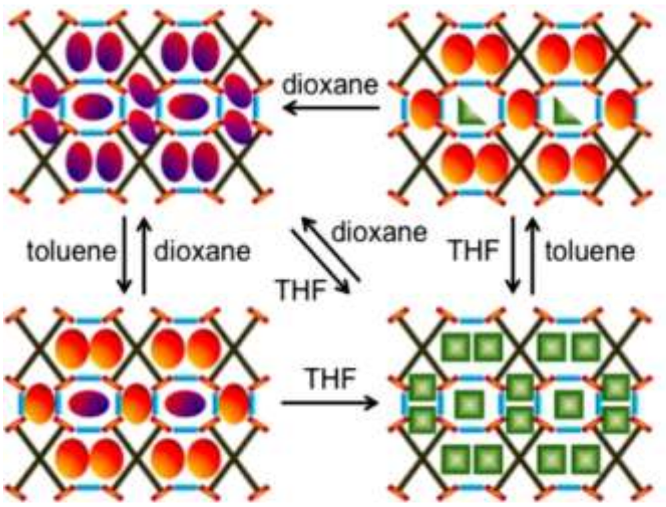

Fig. 25 Schematic illustration of reversible single crystal–single crystal transformations based on G4TSPB framework. Reprinted with permission.[141] Copyright 2014 American Chemical Society.

Except the variation of the ligand length to get isoreticular structures with tunable pore size, another approach involving replacing the dangling functional groups on the internal pore surface were also proposed, which can not only obtain isostructural HOFs with tunable pore size, but also afford binding sites for guest inclusions. The prototypal HOFs are based on steroidal bis-(*N*-phenyl)ureas (nanoporous steroidal ureas NPSU-2 to 4), derivatives of cholic acid as anion receptors,[143] which exhibits 1D chiral channels with pore sizes of 12–14 Å.[144] In these prototypes, the carbonyl groups act as H-bonding acceptors while the urea groups act as H-bonding donors. Each hydrated steroidal bis-(*N*-phenyl)ureas connects to four adjacent steroids through multiple N–H···O and O–H···O interactions, helical steroids chain. In 2013, Davis et al. systematically studied a series of steroidal bis-(*N*-phenyl)ureas by altering the terminal groups on interior pore surface, giving over 20 HOFs with tunable pore size range from ~0 to 13.1 Å. Among these HOFs, NPSU-3 exhibits certain permanent porosity as demonstrated by N_2 adsorption at 77 K, giving a relatively low BET surface area of 29 $m^2\ g^{-1}$. Some variants with functional groups exposed on the pore surface afford the potential to bind guest molecules. Organic dyes including aniline, chlorobenzene to squalene can be directly adsorbed by these materials from their liquid state (Fig. 26). For example, the aniline molecules in NPSU-3 form hexamers, binding to ester carbonyl groups of the framework with N–H···O (3.33 Å) interactions. In addition, adsorption for organic dyes, the HOF crystals exhibit interesting dichroism feature originated from the alignment of the chromophores.

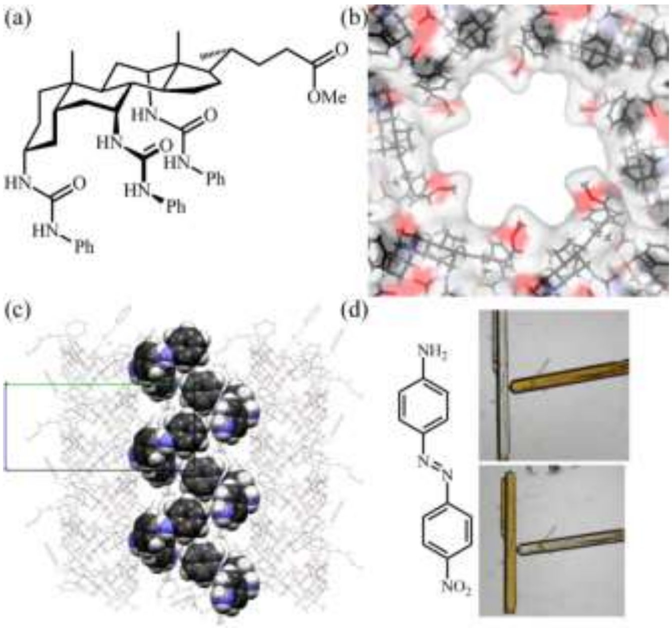

Fig. 26 (a) Methyl 3α,7α,12α-tris[(phenylaminocarbonyl)amino]-5β-cholan-24-oate. (b) Interior surfaces for NPSU-3 viewed along the crystallographic [001] axis. (c) X-ray crystal structure of NPSU-3 with adsorbed aniline, viewed along the crystallographic [001] axis. The aniline is shown in space-filling mode. (d) optical crystals of NPSU-3 with included dyes upon polarized light. For each pair of images the plane of polarization is rotated through 90° between top and bottom. Reprinted with permission.[144] Copyright 2013 American Chemical Society.

Overall, for molecular recognition, the accessible binding sites in HOFs can only interact with substrate through either H-bonds or weak van der Waals forces, showing good reversibility that facilitates the guest release during the regeneration step. On the other hand, porous materials like MOFs with open metal sites can show high selectivity for recognition of different molecules, owing to their strong binding affinity. Apparently, the lack of strong binding sites in HOFs limits their application on this aspect, which needs to take into account for future HOFs construction.

5. HOFs for conductive application

The proton exchange membrane fuel cell (PEMFC) technology for alternative sources of energy is of particular interest, owing to their highly efficient transportation and low-cost maintenance. Porous materials like MOFs have been demonstrated as good proton conductors in related applications, as they are highly porous and easy functionalized that enable them to provide and accommodate various proton carriers. From structural viewpoint, the building units and H-bonding connections in HOFs render them as ideal conducting materials. To be specific, the H-bonded donors/acceptors groups of building units can serve as proton source or carriers, while the widespread H-bonds provide diverse proton transportation pathway. The features of flexibility and solution processability for HOFs open up new possibilities for membrane fabrication, giving light-weight proton-conducting solid electrodes.

To facilitate water-mediated proton-conducting, it is suggested to construct ionic backbones as good proton source, while the open channels can accommodate water molecules as proton carriers. Several types of porous organic salts can be utilized, namely guanidinium−sulfonate HOFs, organic ammonium−sulfonate HOFs. Another advantage for HOFs as conductors is that most HOFs are humidity stable, facilitating for proton conducting. In contrast, most MOFs are unstable upon humidity exposure.

To realize high proton conduction in HOFs, permanently porous frameworks composed of potential proton carrier is applicable. In 2016, we reported a porphyrin-based porous HOF for the application of proton conduction (Fig. 27), which is assembled from 5,10,15,20-tetrakis(4-(2,4-diaminotriazinyl)phenyl)porphyrin (H_2TDPP).[145] In this HOF, (H_2TDPP)·6DMF·5THF (HOF-6), each H_2TDPP connects with eight adjacent ligands through two types of binding models between DAT-DAT moieties with N–H···O (~3.0 Å) interactions, giving 3D 4,4-connected network of two-fold interpenetrations. This HOF contains 3D intersected pore channels (pore size: ~6.4 and 7.5 Å) with neutral porphyrins exposing on the pore surface, which can serve as proton donors/acceptors. The solvent-accessible void ratio of HOF-6 was estimated to be 63.4%. The BET surface area of desolvated HOF-6a was determined to be 130 m^2 g^{-1} based on the CO_2 sorption isotherm at 195 K, confirming its permanent porosity. The proton conductivity of HOF-6a was examined based on its solid sample. At 97% RH and at 300 K, the proton conductivity of HOF-6a is measured to be 3.4×10^{-6} S cm^{-1}, which demonstrates HOFs is applicable for proton conducting materials. In addition, HOF-6a also shows selective adsorption CO_2 over N_2.

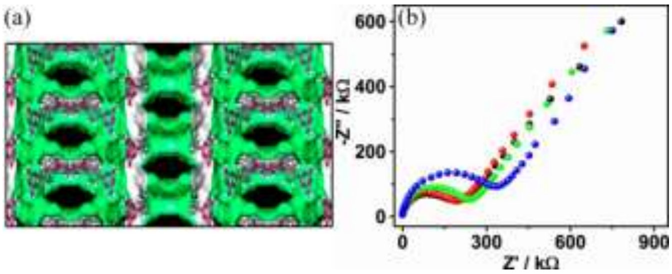

Fig. 27 (a) X-ray crystal structure of HOF-6 indicating 3D packing supramolecular structure along the crystallographic [1,0,1] directions with a channel size of 6.4 Å. (b) Nyquist plots of HOF-6a at 300 K (black), 303 K (red), 308 K (green), and 313 K (blue) in a relative humidity (RH) of 97%. Reprinted with permission.[145] Copyright 2016 American Chemical Society.

Porous guanidinium sulfonate salts might also be good candidates considering their ionic backbones featured with proton source. Although guanidinium sulfonate can form a wide variety of H-bonded structures ranging from clusters, chains to layers, it is still feasible to control their pore structures based on the variation of aromatic moieties. By virtue of guanidinium aryl sulfonate salts, Ghosh *et al.* reported two bilayered porous HOFs,[146] HOF-GS-10 for (G_2NDS)·*x*G (G = guanidinium, NDS^{2-} = 1,5-napthalenedisulfonate) and HOF-GS-11 for previously reported (G_2BPDS)·*x*G[140] (BPDS = 4,4'-Biphenyldisulfonate), that show high proton conduction under humidified conditions (Fig. 28).

In HOF-GS-10, each disulfonate connects with six adjacent guanidinium cations from two guanidinium-sulfonate sheets by using all its oxygen atoms through charge assisted N–H···O (2.90–2.94 Å) interactions, while each guanidinium cation connects with three disulfonate, giving 2D honeycomb-like double-layered network. HOF-GS-11 contains similar bilayer structure with shifted ribbon H-bonding sheets rather than quasihexagonal sheet. Both HOFs exhibit certain permanent porosity as demonstrated by their CO_2 adsorption isotherms at 195 K. Water sorption studies revealed that HOF-GS-10 shows water uptake of 3.47 mmol g^{-1}, while that for HOF-GS-11 is up to 11.6 mmol g^{-1}. Given the coherent H-bonding network and porosity, both HOFs are applied to solid-state proton conducting under humid conditions. At 95% RH and at 303 K, the proton conductivities of HOF-GS-10 and HOF-GS-11 are up to 0.75×10^{-2} and 1.8×10^{-2} S cm−1, which is comparable to those of MOFs. In addition, these compounds also show low activation energy (0.13 eV for HOF-GS-11 vs 0.16 eV for PCMOF-5),[146] further highlight HOFs as promising lightweight materials for fuel-cell technologies.

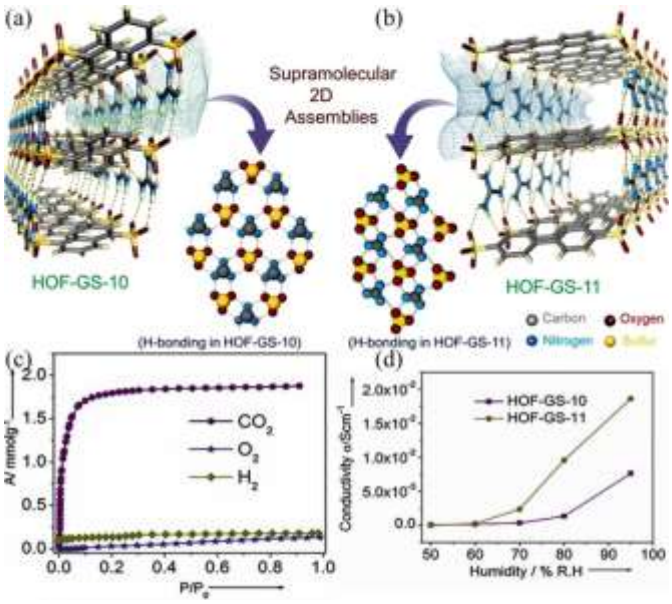

Fig. 28 (a-b) Hydrogen-bonded 2D frameworks of HOF-GS-10 and HOF-GS-11 showing the hydrogen-bonding interaction between the sulfonate groups and the guanidinium cations in both the compounds. (c) CO_2 (dots), O_2 (stars), and H_2 (diamonds) adsorption isotherms of HOF-GS-10 at 195 K (CO_2 and O_2) and at 77 K (H_2). (d) proton conduction values of HOF-GS-10 and HOF-GS-11 at varying humidity and at 303 K. Reproduced with permission.[146] Copyright 2016 Wiley-VCH.

The binding strength of organic linkers is also important for the application of HOFs in proton conducting. For the construction of stable porous organic salts, the acidity/basicity of organic ligands has been proposed as an important factor, referring to the favorable combination of strong acids with strong bases. Recently, Ben *et al.* reported several crystalline porous organic salts (CPOSs)[109,147] featuring high proton conductivity by the combinations of different tetra-acids and diamines (Fig. 29), which reveals such synthesis strategy shows highly correlation with the stability of HOFs. All these four HOFs show total net charge of zero owing to their composition of acid with base in 1:2 ratios, namely CPOS-1 for $(C_6H_{16}N_2)_2(C_{25}H_{16}O_{12}S_4)\cdot 4H_2O$, CPOS-2 for $(C_6H_{10}N_2)_2(C_{25}H_{16}O_{12}S_4)(H_2O)_2\cdot 5H_2O$, CPOS-3 for $(C_{12}H_{14}N_2)_2(C_{25}H_{16}O_{12}S_4)\cdot 2H_2O$ and CPOS-4 for $(C_6H_{16}N_2)_2(C_{29}H_{16}O_8)\cdot 4H_2O$. In these HOFs, two types of ligands are connected to each other by 1D H-bonding chains, giving 3D networks that contain one dimensional chains, clusters or isolated molecules of water. The guest water molecules in these HOFs can be removed below 473 K. The surface area of desolvated CPOS-1 to CPOS-4 were determined to be 216, 129, 12 and 29 m^2 g^{-1} based on the CO_2 sorption isotherm at 273 K by Dubinin–Astakhov method, which demonstrate the combination of relatively strong acid and base helps to improve the framework stability for high pore surface area. The H-bonding chains of charge-assisted N–H···O interactions in the framework and/or guest water molecules can dramatically facilitate the proton conductivity. At 98% RH and at 333 K, the proton conductivities of CPOS-1 to CPOS-4 are up to 1.0×10^{-2}, 2.2×10^{-2}, 3.3×10^{-4} and 7.4×10^{-4} S cm−1, which is proportional to their water contents and the number of corresponding proton carriers. The activation energies of these HOFs reveal that the vehicular mechanism accounts for their proton conduction.

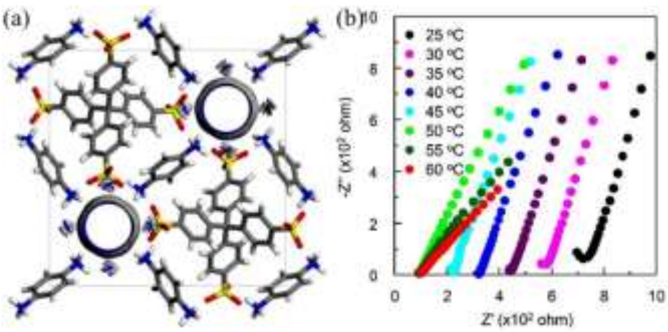

Fig. 29 (a) The 3D porous structure of CPOS-2 showing 1D channels and (b) Temperature dependent proton conductivity of CPOS-2 1-4 at 98% RH. Reproduced with permission.[109] Copyright 2018 Wiley-VCH.

As demonstrated by the above examples, for water-media proton conduction, the proton conductivity of HOFs are comparable to the highly conductive MOFs and commercialized Nafion membranes. The first pioneering works provide some inspirations to further exploration of high conductive HOFs. HOFs for proton conduction are still rarely explored, and many aspects in such application have never been involved. Given the intrinsic advantages of low density, crystalline nature, good processability, especially high intensity of proton carriers, HOFs can serve as new lightweight organic materials for fuel-cell technologies in the field of alternative energy.

6. HOFs for optical applications

As pure organic materials, HOFs are assembled from rationally designed H-bonded motifs. To construct HOFs with permanent porosity, their building blocks are usually designed to be highly rigid molecules featuring aromatic moieties of large π-conjugated system, which usually are excellent fluorescent and phosphorescent dyes, highlighting HOFs as very promising luminescent materials. Depended on the degree of π-conjugation, the emission wavelengths of these organic molecules can distribute over a wide range, facilitating the rational design of luminescent HOF materials with tunable colors. Furthermore, the highly crystalline nature of HOFs indicates the highly ordered arrangement of organic chromophores, giving significantly different emission behaviours as compared to their solution states, such as aggregation induced emission (AIE). In crystalline state, the lumophores are subject to constraints from the lattice and cetain intermolecular close contacts, resulting in spectral shifts, loss of vibronic structure, broadening in the emission, and increased emission lifetimes. In addition, the widely involved intermolecular interactions including π···π interactions enable electronic interactions (e.g. charge transfer) between the lumophores, giving a change in luminescence. Combined the permanent porosity of HOFs accessible for guest species, luminescent sensing can be readily achieved on the basis of host-guest interactions. Consequently, HOFs show great potential for optical applications, which have been rarely shown and only by few examples.

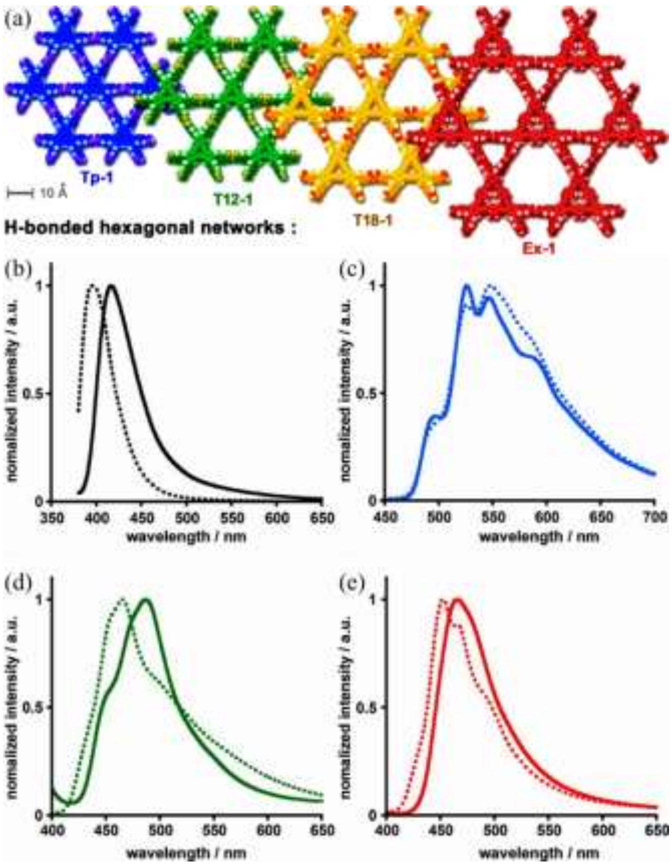

Fig. 30 (a) Crystal structures of H-HexNet motifs of Tp-1, T12-1, T18-1, and Ex-1. Normalized solid state fluorescence spectra of (b) Tp-apo (solid line) and Tp-2Ds (dashed line), (c) T12-apo (solid line) and T12-1 (dashed line), (d) T18-apo-II (solid line) and T18-1 (dashed line), and (e) Ex-apo (solid line) and Ex-1(dashed line). Reprinted with permission.[97] Copyright 2016 American Chemical Society.

Large π-conjugated planar moieties have been widely explored for the construction of permanently porous HOFs owing to their high rigidity, which are also good lumophores of highly luminescent materials.[148,149] Hisaki and co-workers have developed a series of robust HOFs with remarkable porosity and surface area using various C_3-symmetric polycarboxylic acids,[100-102,150,151] referring to triphenylene (Tp), hexadehydrotribenzo[12]annulene (T12), dodecadehydro-tribenzo-[18]annulene (T18), and expanded cyclic phenylene ethynylene (Ex) derivatives (Fig. 30).[97] Each hexacarboxylic acid connects to six adjacent ligands via six -COOH dimers with multiple O–H···O interactions, giving 2D hexagonal network. Each H-bonded layer further stacks with adjacent layers through π···π and C–H···π interactions, showing open framework with two types of accessible pores (triangular and nonregular hexagonal shapes) with sizes of ~11 Å in diameter and 2–11.4 × 15.8 Å^2, respectively. The solvent-accessible void ratios of these HOFs were estimated to be 54% for Tp-1, 41% for T12-1, 58% for T18-1, and 59% for Ex-1. These HOFs show high thermal stability up to 513–633 K. After desolvation, these HOFs exhibit certain structural transformations. Their BET surface areas were estimated to be 557–788 m^2 g^{-1}. These HOFs show different fluorescence spectra with maxima at 416–546 nm, with quantum yields of 5.5–25%. These HOFs also show high uptake capacity for several hydrocarbons.

Another rigid π-conjugated heterocyclic moiety, hexaazatriphenylene (HAT), was also applied to construct rigid and stable HOFs, showing interesting anisotropic single-crystal fluorescence. Using a HAT derived ligand, hexakis(4-carboxyphenyl)-hexaazatriphenylene (CPHAT), with twisted conformation, a 3D rigid HOF (CPHAT-1) can be assembled.[98] This HOF can be simplified as **pcu** topology with 4-fold interpenetration, showing a solvent-accessible void ratio of 31% with pore size of 6.7–8.8 Å in diameter. The BET surface area of CPHAT-1a was estimated to be 649 m^2 g^{-1} based on the CO_2 sorption isotherm at 195 K. This HOF shows remarkable thermal and chemical stability, even in hot water and acid aqueous solution. CPHAT-1a shows a fluorescence emission maximum at 460 nm, and the quantum efficiency is 1.6%. CPHAT-1a shows highly anisotropic emission with anisotropy of 0.65 for perpendicular orientation and -0.32 for parallel orientation, which reveals preferential orientation of the molecular dipole moments in the specific direction.

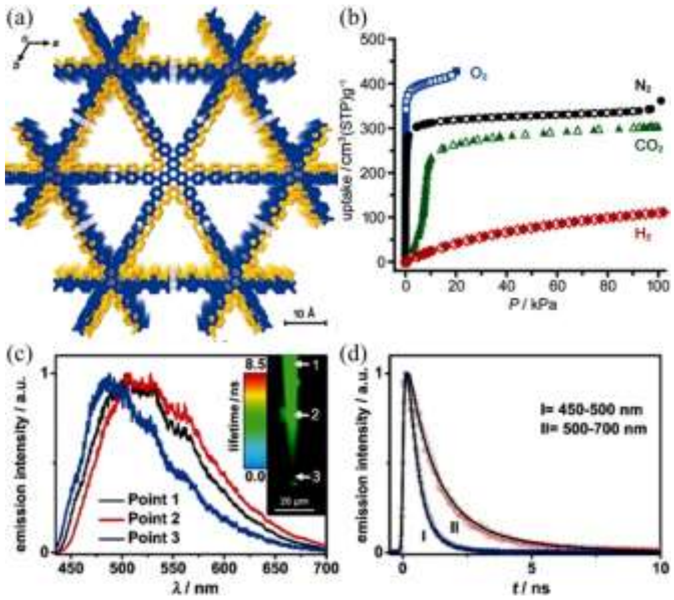

Fig. 31 (a) Packing diagram of CBPHAT-1. (b) Gas sorption isotherms of CBPHAT-1a: O_2 (77 K), N_2 (77 K), CO_2 (195 K), H_2 (77 K). (c) Emission spectra at different points of a CBPHAT-1a crystal. The inset shows an image of the crystal and the points of measurement. (d) Fluorescence decays of a CBPHAT-1a crystal at different spectral regions of the emission spectrum. Reproduced with permission.[99] Copyright 2018 Wiley-VCH.

Recently, Hisaki and Douhal *et al.* reported an expanded HAT derivative HOF (CBPHAT-1) showing isoreticular structure with CPHAT-1 (Fig. 31).[99] CBPHAT-1 exhibits six-fold interpenetrated frameworks with **pcu** topology, with solvent-accessible void ratio of 45% and pore size of 14.5 Å in diameter. The framework of this HOF can retain even up to 578 K as revealed by its variable temperature PXRD patterns. This HOF is stable in boiling water and conc. HCl. The BET surface area of CBPHAT-1a was estimated to be 1288 m^2 g^{-1} based on the N_2 sorption isotherm at 77 K. CBPHAT-1a shows a green-yellow emission with emission maximum at 500 nm, and the quantum efficiency is 5.7%. CBPHAT-1a also shows highly anisotropic emission with anisotropy of 0.45 and -0.30 for perpendicular and parallel orientation, respectively, which is owing to direction-dependent intermolecular interactions originated from oriented molecular stacking. The crystal of CBPHAT-1a shows position-dependent emissions caused by structural defects. These works from the same group well demonstrated the highly ordered crystalline structure in HOFs can generate unique organic luminescence that is distinct from those of dispersed molecules. The above two examples also represent another isoreticular example for construction of HOFs.

To obtain long-lifetime organic phosphorescence, an efficient approach is to embed phosphors into rigid crystalline lattice and thus reduces nonradiative decay of related triplet excitons. Recently, An and Huang *et al.* reported two phosphorescent HOFs (MA-IPA and MA-TPA) composed of melamine (MA) and aromatic acids, which show high phosphorescent efficiencies and ultralong lifetimes (Fig. 32).[152] In both HOFs, the MA molecules are protonated as HMA^+, which connect with deprotonated dicarboxylate moieties and water molecules through strong N–H···O, O–H···N, N–H···N and O–H···O interactions, giving H-bonded ribbons and sheets. Extra interlayer H-bondings, van der Waals force, electrostatic interactions between these secondary structures enable dense packing of these organic phosphors. Notably, all the H-bonding donors and acceptors are fully involved into H-bonding interactions. Therefore, strong photoluminescence of MA-IPA can be observed upon UV excitation, referring emission peaks at ~356 and 466, 488 nm that can be assigned to fluorescence and phosphorescence, respectively. Typically, under suitable UV light, the excitation of organic molecules in HOFs occurs through the spin-allowed singlet–singlet transition, followed by fluorescence emission as direct radiative decay from the lowest singlet excited state and/or phosphorescence emission after intersystem crossing to triplet excitons. The latter usually features rapid nonradiative decay rate, resulting in poor efficiency. With multiple constraints from lattice of HOFs including H-bonding interactions, the nonradiative transition can be suppressed, thus giving highly efficient phosphorescence. The phosphorescence lifetime of MA-IPA is up to 1.91 s, accompanied by a high quantum efficiency of 24.3%, while those of MA-TPA were measured to 1.09s and 19.4% (maximum at 509 nm). This type of HOF materials was also applied for barcode identification in darkness. This work shows that HOF materials are superior in the developing of long-lifetime organic phosphors.

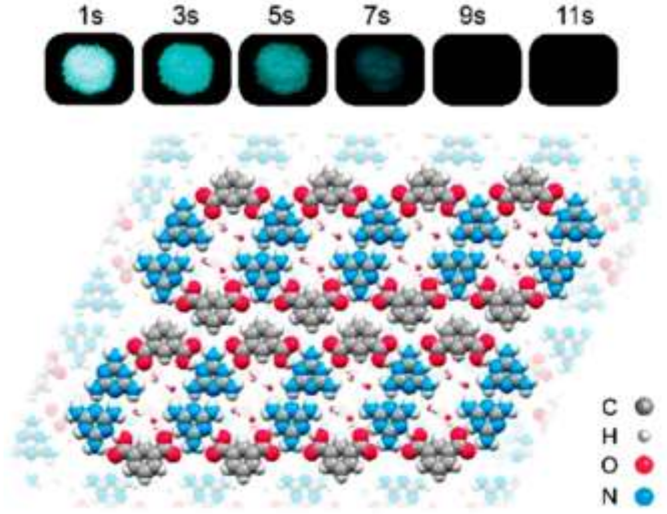

Fig. 32 Schematic representation of supramolecular architecture in MA-IPA showing ultralong organic phosphorescence. Reprinted with permission.[152] Copyright 2018 American Chemical Society.

Tetraphenylethylene (TPE) is promising organic chromophore as it can give aggregation induced emission (AIE) for various applications ranging from chemical sensing to cell imaging. Xie and Chen *et al.* reported a fluorescent HOF (HOF-1111) that composed of DAT-derived ligand with TPE moiety, for fluorescence sensing of aromatic compounds.[153] In this HOF, each TPE-DAT_4 ligand connects to four adjacent intralayer ligands via multiple N–H···N (2.93–3.15 Å) interactions, giving 2D H-bonded layers. Each layer is further linked to a adjacent layer by DMSO and water molecules through N–H···O and O–H···O interactions, giving double-layered structure. This HOF shows potential solvent-accessible void ratio of ~40% with pore size of 6.8 × 10.9 $Å^2$. This HOF exhibits fluorescence emission with maximum at 524 nm. Upon exposure to the vapours of several nitroaromatics, the fluorescence of this HOF was quenched with efficiency up to 73%, showing the potential for detection of nitroaromatic explosives. In contrast, for the vapours of benzene, toluene, *p*-xylene, and trimethylbenzene, enhancements of fluorescence intensity can be observed.

By virtue of suitable binding site, ion species can also be detected by luminescent HOFs. We have demonstrated that selective fluorescence sensing of metal ions can be achieved by using two fluorescent HOFs (HOF-5 and HOF-10) functionalized with DAT moieties.[154] In both two HOFs, besides those H-bonding donors/acceptors for the construction of framework, there are residual sites binding with solvent guest molecules through N–H···O interactions, which are proposed to be binding sites for metal ions during fluorescence sensing. Each TPE-derived ligand in HOF-10 connects to six adjacent ligands and eight DMSO molecules, while that in HOF-5 connects to eight adjacent ligands, two DMF and two DMSO molecules. Theoretically, the potential solvent-accessible void ratio can be up to 55% in HOF-10 and 56% in HOF-5. The BET surface area of desolvated HOF-10a was determined to be 187 $m^2\ g^{-1}$ based on the CO_2 sorption isotherm at 195 K. Upon excitation at 360 nm, HOF-10 and HOF-5 display blue fluorescence emissions with maximums at 468 and 474 nm, respectively, with quantum yields of 0.52 for HOF-10 and 0.63 for HOF-5. After immersion in the solution of 5.0 mM $AgNO_3$, both samples exhibit yellow-green fluorescence with maximums at 502 and 504 nm, accompanied by a color change to pale yellow. In contrast, for Ca^{2+}, Cd^{2+}, Co^{2+}, Cu^{2+}, Mn^{2+},Na^{+}, Ni^{2+} and Zn^{2+}, negligible emission shits can be observed, demonstrating the highly selective sensing for Ag^{+} ions. The binding of Ag^{+} ions to the N atoms of DAT moieties is regarded to account for such selective fluorescence sensing behavior.

Overall, HOFs show great potential in various optical applications, considering they integrate the merits of organic chromophores and permanent porosity into the frameworks. The rigid π-conjugated moieties can serve not only as scaffolds of pore structure but also as luminescent centers. On the other hand, the highly crystalline nature of HOFs facilitates the reduction of nonradiative decays. The initial endeavors including the applications of HOFs as light emitting materials and for fluorescence sensing have demonstrated these advantages. Strong progresses of HOFs in this important application can be expected upon continuous research endeavors.

7. HOFs for other applications

Although HOFs are still in their early stage, some attempts for very promising applications have been carried out, which dramatically highlighted HOFs as emerging porous materials. The advantages that HOFs distinguished from other porous materials are not fully revealed. Given that HOFs are assembled from organic motifs in a reversible binding manner, further applications to make use such feature can be expected. Presumably, the major challenge lies in the stability of HOFs.

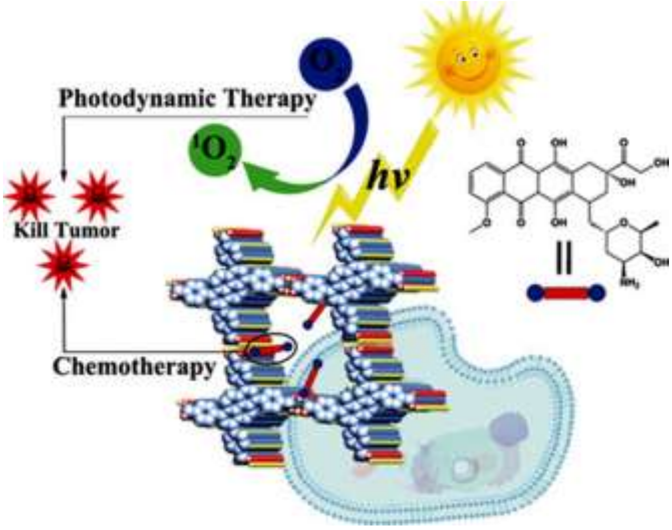

Fig. 33 Schematic diagram of PFC-1 for synergetic chemo-photodynamic therapy by combining the delivery of doxorubicin and generation of singlet oxygen species. Reproduced with permission.[115] Copyright 2018 Wiley-VCH.

Considering HOFs are intrinsically metal-free porous media, their considerable biocompatibility and high porosity render them as excellent candidates for drug delivery and biomedical applications. Recently, Liu and Cao *et al.* reported a stable HOF PFC-1 constructed from 1,3,6,8-tetrakis(p-benzoic acid)pyrene (H_4TBAPy) for chemo-photodynamic therapy, which shows good therapeutic efficacy and low cytotoxicity (Fig. 33).[115] The organic ligand H_4TBAPy was targeted owing to its planar core of large π-conjugated system for extra π···π interactions, which contribute major to the framework stability. In this HOF, each H_4TBAPy ligand connects to six adjacent ligands via four -COOH dimers with multiple strong O–H···O (2.60 Å) interactions, giving 2D uninodal 4-connected **sql** network. Each H-bonded layer further stacks with adjacent layers through strong π···π interactions (3.34 Å), showing open framework with 1D channels of 18 × 23 $Å^2$. The BET surface area of PFC-1 was estimated to be 2122 $m^2\ g^{-1}$ based on the N_2 sorption isotherm at 77 K. Based on the strong multiple intermolecular interactions, this HOF exhibits remarkable chemical stability upon immersion in water, organic solvents and acidic solution, retaining its porosity under harsh condition. Notably, this HOF can be readily healed from potential thermal damage by simple acid leaching. The metal-free nature, inherent porosity, and chemical stability make PFC-1 a good carrier for the delivery of doxorubicin, showing a loading capacity of 26.5 wt%, which facilitates the chemotherapy on cancer. Simultaneously, the suitable arrangement of pyrene moiety enables this HOF to serve as a good candidate photodynamic therapy (PDT), as it can generate singlet oxygen species monitored by chemical trapping with 9,10-diphenylanthracene. In vitro PDT studies of HeLa cells shows doxorubicin@Nano-PFC-1 exhibits synergetic chemo-photodynamic therapy with the merits of low cytotoxicity, good biocompatibility, and high therapeutic efficacy.

HOFs have also been explored as volatile drug vessels, involving the storage and delivery of general inhalation anesthetics such as enflurane, isoflurane, and halothane. In 2015, Miljanić and co-workers reported a fluorinated trispyrazole HOF ($C_{33}H_{12}F_{12}N_6$) as adsorbents for the capture of fluorinated anesthetics, which is aforementioned for the adsorption of fluorocarbons and chlorofluorocarbons.[155] Simple adsorption studies revealed this HOF can take up 2.14–2.67 moles anesthetic molecules per mole adsorbent, corresponding to 56.7–73.4 wt%. Such adsorption and capture is fast and can be saturated within 3 minutes.

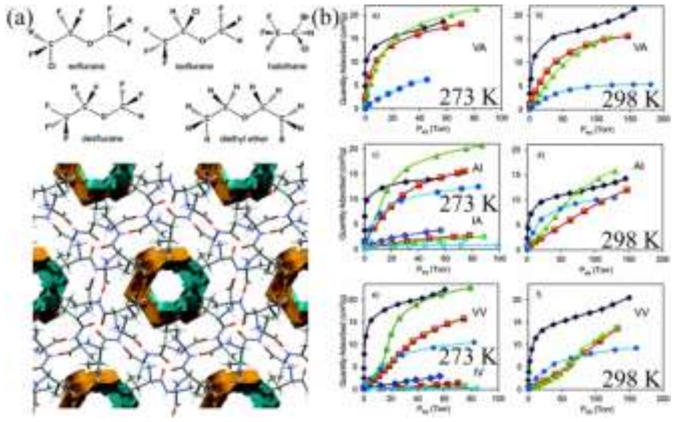

Fig. 34 (a) Chemical structures of the halogenated ethers used as guests (above); portion of the crystal structure of L-valyl-L-alanine (VA) along the channels axis (below). (b) Anesthetics adsorption isotherms in different dipeptides. Reproduced with permission.[156] Copyright 2018, Royal Society of Chemistry.

Later, biocompatible and biodegradable porous sorbents[157] were applied to related applications in medicine. Recently, Sozzani and Comotti *et al.* reported several known nanoporous crystalline peptides for biomedical application involving selective adsorption of a family of volatile anesthetics (Fig. 34).[156] In particular, crystalline dipeptides *L*-alanyl-*L*-isoleucine (AI), *L*-isoleucyl-*L*-alanine (IA), *L*-isoleucyl-*L*-valine (IV) *L*-valyl-*L*-alanine (VA), and *L*-valyl-*L*-valine (VV) are investigated, which feature 1D hydrophobic pore channels with aliphatic side groups exposed on the pore surface. In these HOFs, the amphiphilic dipeptide motifs connect with each other via $NH_3^+\cdots{}^-OOC$ dimers with multiple charge assisted N–H···O (2.70–3.00 Å) and weak C–H···O (3.20–3.41 Å) interactions, giving honeycomb-shaped H-bonded network that contains double helices of dipeptides. These HOFs contains 1D channel with sizes ranging from 3.5 to 5.3 $Å^2$, as modulated by aliphatic groups. The hydrophobic pore structure in these HOFs is beneficial for adsorption of volatile anesthetics namely halogenated ethers and alkanes as revealed by their high adsorption heats. Related vapor adsorption isotherms show that these HOFs can take up 170–200 mmol anesthetic molecules per mole adsorbent at 273 K and 80–100 Torr, corresponding to 20 wt%. The adsorption heats of these HOFs for fluorinated anesthetics are in the range of 35–50 kJ mol^{-1}. Also, ^1H, ^{13}C and ^{19}F MAS NMR coupled with modeling studies were applied to detect the arrangement of adsorbed anesthetics. Therefore, porous HOFs with good biodegradability and biocompatibility are very promising in biomedical applications.

The internal pore cavities of HOFs are also suitable as reaction vessels as long as they possess exchangeable guest-filled voids. Since the arrangement of reactant molecules in porous solids are relatively easy to control compared to those in liquid solutions, controlled reactions with configurational selectivity can be readily expected by using porous solids as reaction vessels. In this respect, HOFs show exceptional ability for cocrystallization or recrystallization with various guest molecules, which highlight them as promising reaction media. An early attempt about stereoselective Diels-Alder reactions promoted by a 2D square grid organic network was performed in 1997.[158] This H-bonded network is composed of anthracenebisresorcinol derivative linked out with four adjacent ligands through O–H···O (2.73 Å) interactions, showing supermolecular sheets with pore cavities. Prior to Diels-Alder reaction, the recrystallization of alkyl acrylates and cyclohexadiene into this network gives single crystal of reactant adduct, showing suitable arrangement of both reactants with ordered interval. Therefore, the acrolein-cyclohexadiene Diels-Alder reaction was performed to show enhanced stereoselectivity.

To improve crystalline order of polymer, Sozzani et al. used nanoporous crystalline peptides as reaction vessels for controlled solid-state polymerization of acrylic or diene monomers in an *in situ* γ-ray-induced manner (Fig. 35).[159] Several porous crystals, namely *L*-alanyl-*L*-valine (Ala-Val), *L*-isoleucyl-*L*-valine (Ile-Val), *L*-valyl-*L*-alanine (Val-Ala), and *L*-valyl-*L*-isoleucine (Val-Ile), are involved, which contain 1D pore channels with sizes of 5.0, 3.9, 4.7 and 3.7 Å in diameters, respectively. Prior to polymerization, the monomer vapors of acrylonitrile, pentadiene, and isoprene were adsorbed into guest-free crystalline peptides, followed by exposure upon γ-ray irradiation for generation of the initiating radicals to promote polymerization. The polymerization at room temperature after one week gives poly(acrylonitrile) (PAN), poly(pentadiene) (PPD) and poly(isoprene) (PI) with molecular weight of 50–150, 20–68 and 100–156 kDa, respectively. Notably, using porous crystal with suitable pore size, the resultant polymer can be isotactic with high stereoregularity demonstrated from corresponding ^{13}C NMR spectra. For isotactic PAN, such topochemical polymerization is achieved under mild conditions of temperature and pressure, which is superior to conventional polymerization methods.

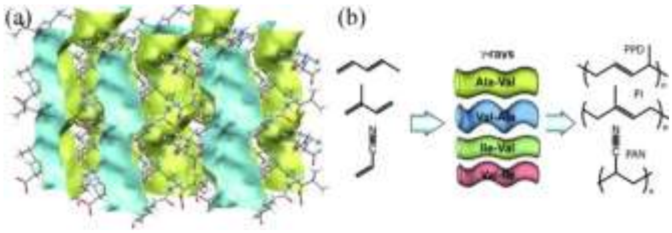

Fig. 35 (a) Crystal structure of porous Ala-Val compound showing the empty channels along the crystallographic [001] axis in blue and yellow. (b) Schematic representation of the monomers and dipeptides used for the polymerization process. Reproduced with permission.[159] Copyright 2012 Wiley-VCH.

Besides serving as reaction vessels, the introduction of functional sites into HOFs render them as catalysts for organic reactions. Li *et al.* reported a cobalt(II) porphyrin HOF (CoTCPp, Co(II) 5,10,15,20-tetra(4-(4-acetateethyl)phenoxy)phenylporphyrin), $(C_{72}H_{44}N_4O_{12})\cdot 2DMF$, for oxidation of alkylbenzenes.[160] In this HOF, each CoTCPp ligand connects to four adjacent ligands via four -COOH dimers with multiple strong O–H···O (2.64–2.68 Å) interactions, giving 2D uninodal 4-connected **sql** network. This HOF contains 1D pore channels (4.0 × 6.5 $Å^2$), showing a solvent-accessible void ratio of 18.9% and a BET surface area of 98 $m^2\ g^{-1}$ estimated from the N_2 sorption isotherm at 77 K. At 353 K in CH_3CN with tertbutylhydroperoxide, the quantitative oxidation of ethylbenzene to acetophenone was achieved with a conversion yield of 83%.

Overall, the intrinsic nature of HOFs renders the type of porous materials attractive for various applications, serving as adsorbents to reaction vessels. There are also attempts to apply HOFs for other applications, e.g. sequestration of radioactive waste like iodine isotopes from aqueous environment.[98] Some interesting dimensions and regions of research have also been performed, involving the post-modification of HOFs to COFs by irreversible organic reactions, which results in new porous organic frameworks of improved stability.[161] Nevertheless, the application potential of HOFs is far more than the above examples, which requires more intersections of different disciplines, involving more practical applications.

8. Conclusions

In this review, we have highlighted the current state of the art for HOFs, including important progresses on their broad application for gas storage and separation, molecular recognition, conductive and optical applications, heterogeneous catalysis, and biomedicine. HOFs are extended porous crystalline frameworks that compose of light-elements organic molecules (mainly C, H, O, N) linked by typical H-bonds. The construction of HOFs with open frameworks can be achieved by the combination of rigid molecular backbones and hydrogen-bonded units with strong intermolecular interactions, while the resultant structures can be further stabilized via introducing interpenetration and other types of intermolecular interactions. The reversible and flexible nature of H-bonding connections enables HOFs to show high crystallinity, solution processability, easy healing and purification. HOFs are intrinsically metal-free and low-density porous media, which can even be biocompatible and biodegradable that are promising for drug delivery and biomedical applications. These features render HOFs as new platform for exploring light-weight functional materials.

As H-bonds are essentially weak interactions featuring poor rigidity and directionality, comparing to zeolites, MOFs and COFs, it is too hard for HOFs to retain their porous framework after the removal of guest molecules. The establishment of microporosity with surface area and pore volume determination has been long-standing challenges since their early developments, and it took a long time to reveal the permanent porosity of HOFs, which initiated the applications of this class of materials as functional porous media. Since the original inception of HOFs, this field rapidly developed, especially in the last few years. In terms of porosity and surface area, substantial progresses have been witnessed, affording the current benchmark HOFs that even comparable to some MOFs of extraordinarily high porosity. Some HOFs show impressive framework stability upon the external stimulus like heat and chemicals, which is even superior to most MOFs. Notably, the healing of HOFs from structural damages can be readily achieved by simple solution processing. Following continuous research endeavours on HOF chemistry, the appearance of this field is expected to change dramatically.

Several challenges remain for HOFs. Precise control over pore size and pore chemistry of HOFs rather than empirical approaches are needed to rationally design new functional HOF materials, in the same manner as MOFs and COFs. Simultaneously, the polymorphism issue during the construction of HOFs needs to be overcome, not only for the phase purity but also for directional synthesis in a predictable way. Also, there are also challenges lie in the construction of outperforming HOFs that integrate the merits of ultra-high surface area and high framework rigidity, where new strategies might be required. It should be noted that strong binding sites especially open metal sites render MOFs as unique host materials for some important applications involving various catalysis reactions and highly selective recognition of molecules. In contrast, the lack of functional sites especially strong Lewis base/acid sites has limited the application of HOFs, which needs to be taken into account during future synthesis and design of HOFs. The last but not the least, intensive efforts will be required for the co-crystallization of mixed organic ligands into single HOFs, either the same type of ligand or different types, though very challenging it can drastically boost the diversity of HOF structures.

More and more research interests have been attracted into this field, owing to the unique features of this class of porous materials. Remarkable evolutions will be brought in the near future. New dimensions and regions of research on HOFs will enrich and supplement the HOF chemistry, which in turns affords diverse functionalities and applications. We see an exciting future for these unique materials.

Conflicts of interest

There are no conflicts to declare.

Acknowledgements

Supports from National Science Foundation (DMR-1606826, B.C.) and the Welch Foundation under Grant AX-1730 (B.C.) are gratefully acknowledged.

Notes and references

1 M. E. Davis, *Nature*, 2002, **417**, 813.

2 A. Corma, *Chem. Rev.*, 1997, **97**, 2373-2420.

3 D. Zhao, J. Feng, Q. Huo, N. Melosh, G. H. Fredrickson, B. F. Chmelka and G. D. Stucky, *Science*, 1998, **279**, 548.

4 J. Li, A. Corma and J. Yu, *Chem. Soc. Rev.*, 2015, **44**, 7112-7127.

5 H. Furukawa, K. E. Cordova, M. O'Keeffe and O. M. Yaghi, *Science*, 2013, **341**, 1230444.

6 S. Kitagawa, R. Kitaura and S.-i. Noro, *Angew. Chem. Int. Ed.*, 2004, **43**, 2334-2375.

7 S. Kitagawa, *Angew. Chem. Int. Ed.*, 2015, **54**, 10686-10687.

8 J. Jiang, Y. Zhao and O. M. Yaghi, *J. Am. Chem. Soc.*, 2016, **138**, 3255-3265.

9 C. S. Diercks and O. M. Yaghi, *Science*, 2017, **355**.

10 X. Feng, X. Ding and D. Jiang, *Chem. Soc. Rev.*, 2012, **41**, 6010-6022.

11 S. Yuan, L. Feng, K. Wang, J. Pang, M. Bosch, C. Lollar, Y. Sun, J. Qin, X. Yang, P. Zhang, Q. Wang, L. Zou, Y. Zhang, L. Zhang, Y. Fang, J. Li and H.-C. Zhou, *Adv. Mater.*, 2018, **30**, 1704303.

12 J.-P. Zhang, H.-L. Zhou, D.-D. Zhou, P.-Q. Liao and X.-M. Chen, *National Sci. Rev.*, 2017, doi: 10.1093/nsr/nwx1127.

13 B. F. Hoskins and R. Robson, *J. Am. Chem. Soc.*, 1989, **111**, 5962-5964.

14 M. Kondo, T. Yoshitomi, H. Matsuzaka, S. Kitagawa and K. Seki, *Angew. Chem. Int. Ed.*, 1997, **36**, 1725-1727.

15 H. Li, M. Eddaoudi, T. L. Groy and O. M. Yaghi, *J. Am. Chem. Soc.*, 1998, **120**, 8571-8572.

16 R.-B. Lin, S. Xiang, B. Li, Y. Cui, W. Zhou, G. Qian and B. Chen, *Israel Journal of Chemistry*, 2018, **58**, 949-961.

17 B. Li, H.-M. Wen, Y. Cui, W. Zhou, G. Qian and B. Chen, *Adv. Mater.*, 2016, **28**, 8819-8860.

18 C. H. Hendon, A. J. Rieth, M. D. Korzyński and M. Dincă, *ACS Cent. Sci.*, 2017, **3**, 554-563.

19 J.-R. Li, R. J. Kuppler and H.-C. Zhou, *Chem. Soc. Rev.*, 2009, **38**, 1477-1504.

20 Z. Bao, G. Chang, H. Xing, R. Krishna, Q. Ren and B. Chen, *Energy Environ. Sci.*, 2016, **9**, 3612-3641.

21 K. Adil, Y. Belmabkhout, R. S. Pillai, A. Cadiau, P. M. Bhatt, A. H. Assen, G. Maurin and M. Eddaoudi, *Chem. Soc. Rev.*, 2017, **46**, 3402-3430.

22 R.-B. Lin, S. Xiang, H. Xing, W. Zhou and B. Chen, *Coord. Chem. Rev.*, 2019, **378**, 87-103.

23 X. Zhao, Y. Wang, D.-S. Li, X. Bu and P. Feng, *Adv. Mater.*, 2018, **30**, 1705189.

24 R.-B. Lin, S.-Y. Liu, J.-W. Ye, X.-Y. Li and J.-P. Zhang, *Adv. Sci.*, 2016, **3**, 1500434.

25 L. Jiao, Y. Wang, H.-L. Jiang and Q. Xu, *Adv. Mater.*, 2017, **30**, 1703663.

26 T. Simon-Yarza, A. Mielcarek, P. Couvreur and C. Serre, *Adv. Mater.*, 2018, **30**, 1707365.

27 K. Lu, T. Aung, N. Guo, R. Weichselbaum and W. Lin, *Adv. Mater.*, 2018, **30**, 1707634.

28 Y. He, S. Xiang and B. Chen, *J. Am. Chem. Soc.*, 2011, **133**, 14570-14573.

29 J. Lü and R. Cao, *Angew. Chem. Int. Ed.*, 2016, **55**, 9474-9480.

30 M. I. Hashim, C. W. Hsu, H. T. M. Le and O. S. Miljanić, *Synlett*, 2016, **27**, 1907-1918.

31 Y.-F. Han, Y.-X. Yuan and H.-B. Wang, *Molecules*, 2017, **22**, 226.

32 J. Luo, J.-W. Wang, J.-H. Zhang, S. Lai and D.-C. Zhong, *CrystEngComm*, 2018, **20**, 5884-5898.

33 M. Simard, D. Su and J. D. Wuest, *J. Am. Chem. Soc.*, 1991, **113**, 4696-4698.

34 D. Venkataraman, S. Lee, J. Zhang and J. S. Moore, *Nature*, 1994, **371**, 591.

35 X. Wang, M. Simard and J. D. Wuest, *J. Am. Chem. Soc.*, 1994, **116**, 12119-12120.

36 K. Endo, T. Sawaki, M. Koyanagi, K. Kobayashi, H. Masuda and Y. Aoyama, *J. Am. Chem. Soc.*, 1995, **117**, 8341-8352.

37 S. V. Kolotuchin, E. E. Fenlon, S. R. Wilson, C. J. Loweth and S. C. Zimmerman, *Angew. Chem. Int. Ed.*, 1996, **34**, 2654-2657.

38 Y. Aoyama, K. Endo, T. Anzai, Y. Yamaguchi, T. Sawaki, K. Kobayashi, N. Kanehisa, H. Hashimoto, Y. Kai and H. Masuda, *J. Am. Chem. Soc.*, 1996, **118**, 5562-5571.

39 P. Bhyrappa, S. R. Wilson and K. S. Suslick, *J. Am. Chem. Soc.*, 1997, **119**, 8492-8502.

40 P. Brunet, M. Simard and J. D. Wuest, *J. Am. Chem. Soc.*, 1997, **119**, 2737-2738.

41 K. Kobayashi, T. Shirasaka, A. Sato, E. Horn and N. Furukawa, *Angew. Chem. Int. Ed.*, 1999, **38**, 3483-3486.

42 J.-H. Fournier, T. Maris, J. D. Wuest, W. Guo and E. Galoppini, *J. Am. Chem. Soc.*, 2003, **125**, 1002-1006.

43 P. Brunet, E. Demers, T. Maris, G. D. Enright and J. D. Wuest, *Angew. Chem. Int. Ed.*, 2003, **42**, 5303-5306.

44 K. Kobayashi, A. Sato, S. Sakamoto and K. Yamaguchi, *J. Am. Chem. Soc.*, 2003, **125**, 3035-3045.

45 M. E. Perron, F. Monchamp, H. Duval, D. Boils-Boissier and J. D. Wuest, *Pure Appl. Chem.*, 2004, **76**, 1345-1351.

46 J. D. Wuest, *Chem. Commun.*, 2005, 5830-5837.

47 N. Malek, T. Maris, M. Simard and J. D. Wuest, *J. Am. Chem. Soc.*, 2005, **127**, 5910-5916.

48 O. Saied, T. Maris, X. Wang, M. Simard and J. D. Wuest, *J. Am. Chem. Soc.*, 2005, **127**, 10008-10009.

49 N. Malek, T. Maris, M.-È. Perron and J. D. Wuest, *Angew. Chem. Int. Ed.*, 2005, **44**, 4021-4025.

50 C. H. Görbitz, M. Nilsen, K. Szeto and L. W. Tangen, *Chem. Commun.*, 2005, 4288-4290.

51 W. Yang, A. Greenaway, X. Lin, R. Matsuda, A. J. Blake, C. Wilson, W. Lewis, P. Hubberstey, S. Kitagawa, N. R. Champness and M. Schröder, *J. Am. Chem. Soc.*, 2010, **132**, 14457-14469.

52 M. Mastalerz and I. M. Oppel, *Angew. Chem. Int. Ed.*, 2012, **51**, 5252-5255.

53 A. Pulido, L. Chen, T. Kaczorowski, D. Holden, M. A. Little, S. Y. Chong, B. J. Slater, D. P. McMahon, B. Bonillo, C. J. Stackhouse, A. Stephenson, C. M. Kane, R.

Clowes, T. Hasell, A. I. Cooper and G. M. Day, *Nature*, 2017, **543**, 657.

54 E. Arunan, G. R. Desiraju, R. A. Klein, J. Sadlej, S. Scheiner, I. Alkorta, D. C. Clary, R. H. Crabtree, J. J. Dannenberg, P. Hobza, H. G. Kjaergaard, A. C. Legon, B. Mennucci and D. J. Nesbitt, *Pure Appl. Chem.*, 2011, **83**, 1637-1641.

55 T. Steiner, *Angew. Chem. Int. Ed.*, 2002, **41**, 48-76.

56 H. R. Allcock and L. A. Siegel, *J. Am. Chem. Soc.*, 1964, **86**, 5140-5144.

57 P. Sozzani, A. Comotti, R. Simonutti, T. Meersmann, J. W. Logan and A. Pines, *Angew. Chem. Int. Ed.*, 2000, **39**, 2695-2699.

58 P. Sozzani, S. Bracco, A. Comotti, L. Ferretti and R. Simonutti, *Angew. Chem. Int. Ed.*, 2005, **44**, 1816-1820.

59 G. Couderc, T. Hertzsch, N. R. Behrnd, K. Krämer and J. Hulliger, *Microporous Mesoporous Mater.*, 2006, **88**, 170-175.

60 R. M. Barrer and V. H. Shanson, *J. Chem. Soc., Chem. Commun.*, 1976, 333-334.

61 F. Lee, E. Gabe, J. S. Tse and J. A. Ripmeester, *J. Am. Chem. Soc.*, 1988, **110**, 6014-6019.

62 G. O. Lloyd, M. W. Bredenkamp and L. J. Barbour, *Chem. Commun.*, 2005, 4053-4055.

63 J. L. Atwood, L. J. Barbour, A. Jerga and B. L. Schottel, *Science*, 2002, **298**, 1000.

64 J. L. Atwood, L. J. Barbour and A. Jerga, *Angew. Chem. Int. Ed.*, 2004, **43**, 2948-2950.

65 P. K. Thallapally, L. Dobrzańska, T. R. Gingrich, T. B. Wirsig, L. J. Barbour and J. L. Atwood, *Angew. Chem. Int. Ed.*, 2006, **45**, 6506-6509.

66 S. J. Dalgarno, P. K. Thallapally, L. J. Barbour and J. L. Atwood, *Chem. Soc. Rev.*, 2007, **36**, 236-245.

67 P. K. Thallapally, B. P. McGrail, J. L. Atwood, C. Gaeta, C. Tedesco and P. Neri, *Chem. Mater.*, 2007, **19**, 3355-3357.

68 P. K. Thallapally, B. Peter McGrail, S. J. Dalgarno, H. T. Schaef, J. Tian and J. L. Atwood, *Nat. Mater.*, 2008, **7**, 146.

69 W. A. Freeman, W. L. Mock and N. Y. Shih, *J. Am. Chem. Soc.*, 1981, **103**, 7367-7368.

70 S. Lim, H. Kim, N. Selvapalam, K.-J. Kim, S. J. Cho, G. Seo and K. Kim, *Angew. Chem. Int. Ed.*, 2008, **47**, 3352-3355.

71 H. Kudo, R. Hayashi, K. Mitani, T. Yokozawa, N. C. Kasuga and T. Nishikubo, *Angew. Chem. Int. Ed.*, 2006, **45**, 7948-7952.

72 T. Tozawa, J. T. A. Jones, S. I. Swamy, S. Jiang, D. J. Adams, S. Shakespeare, R. Clowes, D. Bradshaw, T. Hasell, S. Y. Chong, C. Tang, S. Thompson, J. Parker, A. Trewin, J. Bacsa, A. M. Z. Slawin, A. Steiner and A. I. Cooper, *Nat. Mater.*, 2009, **8**, 973.

73 N. Giri, M. G. Del Pópolo, G. Melaugh, R. L. Greenaway, K. Rätzke, T. Koschine, L. Pison, M. F. C. Gomes, A. I. Cooper and S. L. James, *Nature*, 2015, **527**, 216.

74 T. Hasell and A. I. Cooper, *Nat. Rev. Mater.*, 2016, **1**, 16053.

75 T. Ogoshi, T.-a. Yamagishi and Y. Nakamoto, *Chem. Rev.*, 2016, **116**, 7937-8002.

76 J. Tian, L. Chen, D.-W. Zhang, Y. Liu and Z.-T. Li, *Chem. Commun.*, 2016, **52**, 6351-6362.

77 S. Cai, H. Shi, Z. Zhang, X. Wang, H. Ma, N. Gan, Q. Wu, Z. Cheng, K. Ling, M. Gu, C. Ma, L. Gu, Z. An and W. Huang, *Angew. Chem. Int. Ed.*, 2018, **57**, 4005-4009.

78 T. Yu, D. Ou, Z. Yang, Q. Huang, Z. Mao, J. Chen, Y. Zhang, S. Liu, J. Xu, M. R. Bryce and Z. Chi, *Chem. Sci.*, 2017, **8**, 1163-1168.

79 I. Hisaki, H. Senga, H. Shigemitsu, N. Tohnai and M. Miyata, *Chem. Eur. J.*, 2011, **17**, 14348-14353.

80 M. Mastalerz, *Chem. Eur. J.*, 2012, **18**, 10082-10091.

81 M. Mastalerz, *Acc. Chem. Res.*, 2018, **51**, 2411-2422.

82 Y. Zhou, B. Liu, X. Sun, J. Li, G. Li, Q. Huo and Y. Liu, *Cryst. Growth Des.*, 2017, **17**, 6653-6659.

83 M. Sanchez-Sala, O. Vallcorba, C. Domingo and J. A. Ayllón, *Cryst. Growth Des.*, 2018, **18**, 6621-6626.

84 H. Wahl, D. A. Haynes and T. le Roex, *Cryst. Growth Des.*, 2017, **17**, 4377-4383.

85 P. Li, P. Li, M. R. Ryder, Z. Liu, C. L. Stern, O. K. Farha and F. Stoddart, *Angew. Chem. Int. Ed.*, 2018, **57**, DOI: 10.1002/anie.201811263.

86 I. Hisaki, S. Nakagawa, Y. Suzuki and N. Tohnai, *Chem. Lett.*, 2018, **47**, 1143-1146.

87 J. Castells-Gil, N. M. Padial and C. Martí-Gastaldo, *New J. Chem.*, 2018, **42**, 16138-16143.

88 T.-H. Chen, I. Popov, W. Kaveevivitchai, Y.-C. Chuang, Y.-S. Chen, O. Daugulis, A. J. Jacobson and O. Š. Miljanić, *Nat. Commun.*, 2014, **5**, 5131.

89 K. E. Maly, E. Gagnon, T. Maris and J. D. Wuest, *J. Am. Chem. Soc.*, 2007, **129**, 4306-4322.

90 K. E. Maly, W. Buck and L. N. Dawe, *CrystEngComm*, 2017, **19**, 6401-6405.

91 X.-Z. Luo, X.-J. Jia, J.-H. Deng, J.-L. Zhong, H.-J. Liu, K.-J. Wang and D.-C. Zhong, *J. Am. Chem. Soc.*, 2013, **135**, 11684-11687.

92 M. Morshedi, M. Thomas, A. Tarzia, C. J. Doonan and N. G. White, *Chem. Sci.*, 2017, **8**, 3019-3025.

93 C. Chaumont, P. Mobian, N. Kyritsakas and M. Henry, *CrystEngComm*, 2013, **15**, 6845-6862.

94 P. Li, O. Alduhaish, H. D. Arman, H. Wang, K. Alfooty and B. Chen, *Cryst. Growth Des.*, 2014, **14**, 3634-3638.

95 L. Liu, Y. Zhang, X.-L. Wang, G.-G. Luo, Z.-J. Xiao, L. Cheng and J.-C. Dai, *Cryst. Growth Des.*, 2018, **18**, 1629-1635.

96 S. J. Makowski, P. Köstler and W. Schnick, *Chem. Eur. J.*, 2012, **18**, 3248-3257.

97 I. Hisaki, S. Nakagawa, N. Ikenaka, Y. Imamura, M. Katouda, M. Tashiro, H. Tsuchida, T. Ogoshi, H. Sato, N. Tohnai and M. Miyata, *J. Am. Chem. Soc.*, 2016, **138**, 6617-6628.

98 I. Hisaki, N. Ikenaka, E. Gomez, B. Cohen, N. Tohnai and A. Douhal, *Chem. Eur. J.*, 2017, **23**, 11611-11619.

99 I. Hisaki, Y. Suzuki, E. Gomez, B. Cohen, N. Tohnai and A. Douhal, *Angew. Chem. Int. Ed.*, 2018, **57**, 12650-12655.

100 I. Hisaki, S. Nakagawa, N. Tohnai and M. Miyata, *Angew. Chem. Int. Ed.*, 2015, **54**, 3008-3012.

101 I. Hisaki, H. Toda, H. Sato, N. Tohnai and H. Sakurai, *Angew. Chem. Int. Ed.*, 2017, **56**, 15294-15298.

102 I. Hisaki, S. Nakagawa, H. Sato and N. Tohnai, *Chem. Commun.*, 2016, **52**, 9781-9784.

103 M. I. Hashim, H. T. M. Le, T.-H. Chen, Y.-S. Chen, O. Daugulis, C.-W. Hsu, A. J. Jacobson, W. Kaveevivitchai, X. Liang, T. Makarenko, O. Š. Miljanić, I. Popovs, H. V. Tran, X. Wang, C.-H. Wu and J. I. Wu, *J. Am. Chem. Soc.*, 2018, **140**, 6014-6026.

104 Y.-H. Luo, X.-T. He, D.-L. Hong, C. Chen, F.-H. Chen, J. Jiao, L.-H. Zhai, L.-H. Guo and B.-W. Sun, *Adv. Funct. Mater.*, 2018, **28**, 1804822.

105 M. Morshedi, J. S. Ward, P. E. Kruger and N. G. White, *Dalton Trans.*, 2018, **47**, 783-790.

106 Y. Manjare, V. Nagarajan and V. R. Pedireddi, *Cryst. Growth Des.*, 2014, **14**, 723-729.

107 J. Lü, C. Perez-Krap, M. Suyetin, N. H. Alsmail, Y. Yan, S. Yang, W. Lewis, E. Bichoutskaia, C. C. Tang, A. J. Blake, R. Cao and M. Schröder, *J. Am. Chem. Soc.*, 2014, **136**, 12828-12831.

108 Y. Li, M. Handke, Y.-S. Chen, A. G. Shtukenberg, C. T. Hu and M. D. Ward, *J. Am. Chem. Soc.*, 2018, **140**, 12915-12921.

109 G. Xing, T. Yan, S. Das, T. Ben and S. Qiu, *Angew. Chem. Int. Ed.*, 2018, **57**, 5345-5349.

110 H. Yamagishi, H. Sato, A. Hori, Y. Sato, R. Matsuda, K. Kato and T. Aida, *Science*, 2018, **361**, 1242.

111 Z. Bao, D. Xie, G. Chang, H. Wu, L. Li, W. Zhou, H. Wang, Z. Zhang, H. Xing, Q. Yang, M. J. Zaworotko, Q. Ren and B. Chen, *J. Am. Chem. Soc.*, 2018, **140**, 4596-4603.

112 F. Hu, C. Liu, M. Wu, J. Pang, F. Jiang, D. Yuan and M. Hong, *Angew. Chem. Int. Ed.*, 2017, **56**, 2101-2104.

113 J. Duan, W. Jin and S. Kitagawa, *Coord. Chem. Rev.*, 2017, **332**, 48-74.

114 J. J. Low, A. I. Benin, P. Jakubczak, J. F. Abrahamian, S. A. Faheem and R. R. Willis, *J. Am. Chem. Soc.*, 2009, **131**, 15834-15842.

115 Q. Yin, P. Zhao, R.-J. Sa, G.-C. Chen, J. Lü, T.-F. Liu and R. Cao, *Angew. Chem. Int. Ed.*, 2018, **57**, 7691-7696.

116 A. Yamamoto, T. Hirukawa, I. Hisaki, M. Miyata and N. Tohnai, *Tetrahedron Lett.*, 2013, **54**, 1268-1273.

117 P. Li, Y. He, H. D. Arman, R. Krishna, H. Wang, L. Weng and B. Chen, *Chem. Commun.*, 2014, **50**, 13081-13084.

118 Q. Ji, H. T. M. Le, X. Wang, Y.-S. Chen, T. Makarenko, A. J. Jacobson and O. Š. Miljanić, *Chem. Eur. J.*, 2015, **21**, 17205-17209.

119 I. Bassanetti, S. Bracco, A. Comotti, M. Negroni, C. Bezuidenhout, S. Canossa, P. P. Mazzeo, L. Marchió and P. Sozzani, *J. Mater. Chem. A*, 2018, **6**, 14231-14239.

120 J. Lü, C. Perez-Krap, F. Trousselet, Y. Yan, N. H. Alsmail, B. Karadeniz, N. M. Jacques, W. Lewis, A. J. Blake, F.-X. Coudert, R. Cao and M. Schröder, *Cryst. Growth Des.*, 2018, **18**, 2555-2562.

121 S. Nandi, D. Chakraborty and R. Vaidhyanathan, *Chem. Commun.*, 2016, **52**, 7249-7252.

122 A. Lenz and L. Ojamäe, *The Journal of Physical Chemistry A*, 2011, **115**, 6169-6176.

123 W. Yang, J. Wang, H. Wang, Z. Bao, J. C.-G. Zhao and B. Chen, *Cryst. Growth Des.*, 2017, **17**, 6132-6137.

124 P. S. Nugent, V. L. Rhodus, T. Pham, K. Forrest, L. Wojtas, B. Space and M. J. Zaworotko, *J. Am. Chem. Soc.*, 2013, **135**, 10950-10953.

125 S. A. Dalrymple and G. K. H. Shimizu, *J. Am. Chem. Soc.*, 2007, **129**, 12114-12116.

126 P. Dechambenoit, S. Ferlay, N. Kyritsakas and M. W. Hosseini, *J. Am. Chem. Soc.*, 2008, **130**, 17106-17113.

127 W. Wei, W. Li, X. Wang and J. He, *Cryst. Growth Des.*, 2013, **13**, 3843-3846.

128 B. H. Wilson, H. S. Scott, O. T. Qazvini, S. G. Telfer, C. Mathonière, R. Clérac and P. E. Kruger, *Chem. Commun.*, 2018, **54**, 13391-13394.

129 J. M. Taylor, P. J. Dwyer, J. W. Reid, B. S. Gelfand, D.-w. Lim, M. Donoshita, S. L. Veinberg, H. Kitagawa, V. N. Vukotic and G. K. H. Shimizu, *Chem*, 2018, **4**, 868-878.

130 H. Wang, B. Li, H. Wu, T.-L. Hu, Z. Yao, W. Zhou, S. Xiang and B. Chen, *J. Am. Chem. Soc.*, 2015, **137**, 9963-9970.

131 W. Yang, B. Li, H. Wang, O. Alduhaish, K. Alfooty, M. A. Zayed, P. Li, H. D. Arman and B. Chen, *Cryst. Growth Des.*, 2015, **15**, 2000-2004.

132 H. Wang, H. Wu, J. Kan, G. Chang, Z. Yao, B. Li, W. Zhou, S. Xiang, J. C.-G. Zhao and B. Chen, *J. Mater. Chem. A*, 2017, **5**, 8292-8296.

133 P. Li, Y. He, Y. Zhao, L. Weng, H. Wang, R. Krishna, H. Wu, W. Zhou, M. O'Keeffe, Y. Han and B. Chen, *Angew. Chem. Int. Ed.*, 2014, **54**, 574-577.

134 C. A. Zentner, H. W. H. Lai, J. T. Greenfield, R. A. Wiscons, M. Zeller, C. F. Campana, O. Talu, S. A. FitzGerald and J. L. C. Rowsell, *Chem. Commun.*, 2015, **51**, 11642-11645.

135 H. W. H. Lai, R. A. Wiscons, C. A. Zentner, M. Zeller and J. L. C. Rowsell, *Cryst. Growth Des.*, 2016, **16**, 821-833.

136 T.-U. Yoon, S. B. Baek, D. Kim, E.-J. Kim, W.-G. Lee, B. K. Singh, M. S. Lah, Y.-S. Bae and K. S. Kim, *Chem. Commun.*, 2018, **54**, 9360-9363.

137 D.-D. Zhou, Y.-T. Xu, R.-B. Lin, Z.-W. Mo, W.-X. Zhang and J.-P. Zhang, *Chem. Commun.*, 2016, **52**, 4991-4994.

138 P. Li, Y. He, J. Guang, L. Weng, J. C.-G. Zhao, S. Xiang and B. Chen, *J. Am. Chem. Soc.*, 2014, **136**, 547-549.

139 W. Yan, X. Yu, T. Yan, D. Wu, E. Ning, Y. Qi, Y.-F. Han and Q. Li, *Chem. Commun.*, 2017, **53**, 3677-3680.

140 J. A. Swift, A. M. Reynolds and M. D. Ward, *Chem. Mater.*, 1998, **10**, 4159-4168.

141 W. Xiao, C. Hu and M. D. Ward, *J. Am. Chem. Soc.*, 2014, **136**, 14200-14206.

142 T. Adachi and M. D. Ward, *Acc. Chem. Res.*, 2016, **49**, 2669-2679.

143 A. L. Sisson, V. del Amo Sanchez, G. Magro, A. M. E. Griffin, S. Shah, J. P. H. Charmant and A. P. Davis, *Angew. Chem. Int. Ed.*, 2005, **44**, 6878-6881.

144 R. Natarajan, L. Bridgland, A. Sirikulkajorn, J.-H. Lee, M. F. Haddow, G. Magro, B. Ali, S. Narayanan, P.

Strickland, J. P. H. Charmant, A. G. Orpen, N. B. McKeown, C. G. Bezzu and A. P. Davis, *J. Am. Chem. Soc.*, 2013, **135**, 16912-16925.

145 W. Yang, F. Yang, T.-L. Hu, S. C. King, H. Wang, H. Wu, W. Zhou, J.-R. Li, H. D. Arman and B. Chen, *Cryst. Growth Des.*, 2016, **16**, 5831-5835.

146 A. Karmakar, R. Illathvalappil, B. Anothumakkool, A. Sen, P. Samanta, A. V. Desai, S. Kurungot and S. K. Ghosh, *Angew. Chem. Int. Ed.*, 2016, **55**, 10667-10671.

147 G. Xing, I. Bassanetti, S. Bracco, M. Negroni, C. Bezuidenhout, T. Ben, P. Sozzani and A. Comotti, *Chem. Sci.*, 2019, **10**, DOI: 10.1039/C1038SC04376K.

148 E. Gomez, M. Gutiérrez, B. Cohen, I. Hisaki and A. Douhal, *J. Mater. Chem. C*, 2018, **6**, 6929-6939.

149 I. Hisaki, N. Q. Emilya Affendy and N. Tohnai, *CrystEngComm*, 2017, **19**, 4892-4898.

150 I. Hisaki, N. Ikenaka, N. Tohnai and M. Miyata, *Chem. Commun.*, 2016, **52**, 300-303.

151 I. Hisaki, N. Ikenaka, S. Tsuzuki and N. Tohnai, *Mater. Chem. Front.*, 2018, **2**, 338-346.

152 L. Bian, H. Shi, X. Wang, K. Ling, H. Ma, M. Li, Z. Cheng, C. Ma, S. Cai, Q. Wu, N. Gan, X. Xu, Z. An and W. Huang, *J. Am. Chem. Soc.*, 2018, **140**, 10734-10739.

153 Z. Sun, Y. Li, L. Chen, X. Jing and Z. Xie, *Cryst. Growth Des.*, 2015, **15**, 542-545.

154 H. Wang, Z. Bao, H. Wu, R.-B. Lin, W. Zhou, T.-L. Hu, B. Li, J. C.-G. Zhao and B. Chen, *Chem. Commun.*, 2017, **53**, 11150-11153.

155 T.-H. Chen, W. Kaveevivitchai, A. J. Jacobson and O. Š. Miljanić, *Chem. Commun.*, 2015, **51**, 14096-14098.

156 S. Bracco, D. Asnaghi, M. Negroni, P. Sozzani and A. Comotti, *Chem. Commun.*, 2018, **54**, 148-151.

157 P. Teng, Z. Niu, F. She, M. Zhou, P. Sang, G. M. Gray, G. Verma, L. Wojtas, A. van der Vaart, S. Ma and J. Cai, *J. Am. Chem. Soc.*, 2018, **140**, 5661-5665.

158 K. Endo, T. Koike, T. Sawaki, O. Hayashida, H. Masuda and Y. Aoyama, *J. Am. Chem. Soc.*, 1997, **119**, 4117-4122.

159 G. Distefano, A. Comotti, S. Bracco, M. Beretta and P. Sozzani, *Angew. Chem. Int. Ed.*, 2012, **51**, 9258-9262.

160 Z. Zhang, J. Li, Y. Yao and S. Sun, *Cryst. Growth Des.*, 2015, **15**, 5028-5033.

161 Y. Lin, X. Jiang, S. T. Kim, S. B. Alahakoon, X. Hou, Z. Zhang, C. M. Thompson, R. A. Smaldone and C. Ke, *J. Am. Chem. Soc.*, 2017, **139**, 7172-7175.

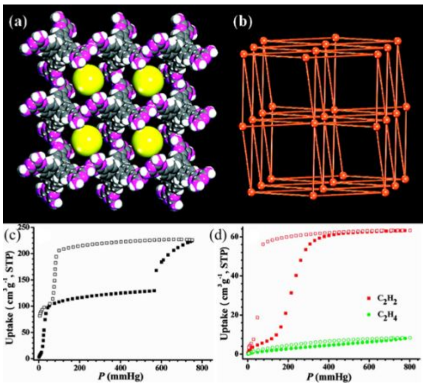

This review provides an overview of development in the design, synthesis, and application of multifunctional porous hydrogen-bonded organic framework (HOF) materials.